

Color it, Code it, Cancel it: k -local dynamical decoupling from classical additive codes

Minh T. P. Nguyen,^{1,*} Maximilian Rimbach-Russ,¹ and Stefano Bosco^{1,†}

¹*QuTech and Kavli Institute of Nanoscience, Delft University of Technology, Lorentzweg 1, 2628 CJ Delft, The Netherlands*

Dynamical decoupling is a central technique in quantum computing for actively suppressing decoherence and systematic imperfections through sequences of single-qubit operations. Conventional sequences typically aim to completely freeze system dynamics, often resulting in long protocols whose length scales exponentially with system size. In this work, we introduce a general framework for constructing time-optimal, selectively-tailored sequences that remove only specific local interactions. By combining techniques from graph coloring and classical coding theory, our approach enables compact and hardware-tailored sequences across diverse qubit platforms, efficiently canceling undesired Hamiltonian terms while preserving target interactions. This opens up broad applications in quantum computing and simulation. At the core of our method is a mapping between dynamical decoupling sequence design and error-detecting codes, which allows us to leverage powerful coding-theoretic tools to construct customized sequences. To overcome exponential overheads, we exploit symmetries in colored interaction hypergraphs, extending graph-coloring strategies to arbitrary many-body Hamiltonians. We demonstrate the effectiveness of our framework through concrete examples, including compact sequences that suppress residual ZZ and ZZZ interactions in superconducting qubits and Heisenberg exchange coupling in spin qubits. We also show how it enables Hamiltonian engineering by simulating the anisotropic Kitaev honeycomb model using only isotropic Heisenberg interactions.

I. INTRODUCTION

Dynamical decoupling (DD), originally inspired by nuclear magnetic resonance [1–5], has become a powerful technique in quantum information processing. Traditionally, DD has been employed to mitigate imperfections in near-term quantum devices by using sequences of single-qubit operations to isolate quantum systems from environmental noise [6–9]. Sequences that suppress on-site decoherence to high order in time include for example universal single-qubit protocols [7, 8], XY family [10–12], concatenated sequences [13, 14], and the Uhrig family [15–17]. DD has also found applications in quantum sensing, such as frequency-selective spectroscopy [18, 19], and in quantum error correction [20, 21].

Beyond decoherence, DD protocols have been effective in suppressing systematic errors originating from high-order qubit interactions, such as residual crosstalk [22–24] from two-body couplings, leading to advanced sequences such as WAHUA [25] and fractal decoupling [26]. However, these methods were designed primarily for small systems with limited connectivity. Recent advances aim to develop time-efficient DD sequences suppressing 2-local interactions for large devices, with sequence length depending only on the topology of the connectivity graphs of the device [24, 27–29]. Moreover, while conventional DD sequences typically freeze the system dynamics entirely, making them difficult to adapt for designing specific quantum evolutions, recent developments have proposed DD protocols for quantum simulation, including the engineering of target Hamiltonians using average Hamiltonian theory [30].

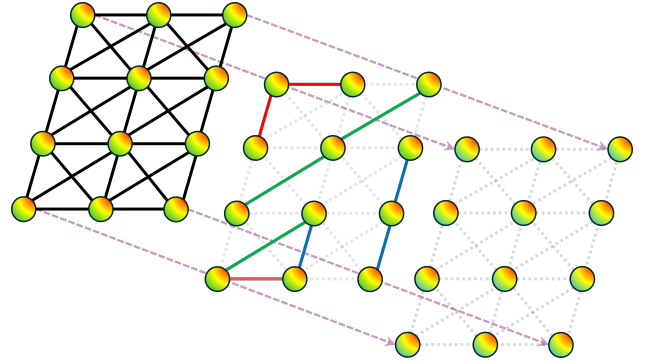


FIG. 1: **Canceling local interactions by dynamical decoupling.** Our framework permits an efficient and selective suppression of local interactions. For example, by applying tailored DD sequences to a device with dense connectivity (top), we can separate the system into non-interacting clusters, preserving only certain interactions within each cluster (middle), or completely freezing the system’s dynamics (bottom). Our framework also applies to general interactions graphs going beyond nearest neighbor and is not restricted to instantaneous control pulses.

In this work, we present a unified framework that enables the systematic construction of time-efficient and robust DD sequences capable of selectively suppressing any chosen k -local interactions, as sketched in Fig. 1. Our framework is built on three key ideas. First, we show that any k -local Hamiltonian induces a hypergraph symmetry that partitions physical qubits into equivalence color classes. This symmetry enables the design of DD sequences that suppress k -local interactions with sequence lengths determined only by the device topology, rather than by system size. This generalizes prior work [24, 27–

* m.t.phamnguyen@tudelft.nl

† s.bosco@tudelft.nl

29], which was limited to 2-local interactions. Second, we exploit the established connection between DD and classical additive codes [31, 32]. This correspondence allows us to identify high-performance DD sequences directly from code parameters and allow us to design hardware-tailored sequences for both superconducting and spin qubit platforms. Furthermore, it opens paths for using DD as a tool in Hamiltonian engineering [30, 33, 34]. Finally, we show how to construct DD sequences based on the underlying group structure that are intrinsically robust to pulse imperfections. Our framework naturally supports finite-width pulses with bounded-strength control [35], eliminating the need for idealized instantaneous (bang–bang) operations [7]. Moreover, the mapping between DD sequences and classical detection codes can potentially enable the use of machine-learning approaches [36–38] by dramatically reducing the search space of candidate sequences and providing an efficient route to generating large, task-specific training datasets.

The flowchart of the framework proposed in this work is summarized in Fig. 2. The manuscript is organized as follows. In Sec. II, we briefly review bang-bang dynamical decoupling, emphasizing the connection between DD sequences and group theory. In Sec. III, we reinterpret the results of Refs. [24, 27] by uncovering a symmetry structure in colored interaction graphs, and extend this perspective to general k -local Hamiltonians. We show that by embedding these symmetries into the group structure of DD sequences, one can construct sequences with lengths depending only on the device topology. In Sec. IV, we introduce the correspondence between DD sequences and classical additive codes, which allows us to characterize the properties of DD sequences directly from code parameters. In Sec. V, we present two applications that explicitly demonstrate the power of our framework: (i) a general time-efficient decoupling protocol for two- and three-local interactions tailored to superconducting and spin qubits, and (ii) a DD sequence permitting quantum simulation of the Kitaev honeycomb model, which strongly relies on anisotropic interactions, using only isotropic Heisenberg exchange interactions. Finally, in Sec. VI, we explain how to construct robust implementations of DD sequences using their group structure, before offering concluding remarks in Sec. VII. While significant room for future improvement remains, our work provides the first systematic framework for constructing scalable DD sequences suitable for near-term quantum devices.

II. DECOUPLING SEQUENCES FROM GROUP THEORY

In this section, we review the basic of dynamical decoupling theory and its formulation in terms of group theory. This section is organized as follows. In Sec. II A, we introduce DD from Floquet theory and the first-order Magnus expansion. In Sec. II B, we formulate dynamical decoupling sequences within a group-theoretic framework.

A. Dynamical decoupling

DD offers a general framework for suppressing unwanted interactions arising from arbitrary Hamiltonians by applying sequences of quantum gates. This approach is traditionally employed in scenarios where a quantum system is weakly coupled to an environment, with the objective that, after the DD sequence, the influence of the environment on the system is effectively canceled. In particular, we consider the Hamiltonian [7]

$$H_{tot} = H_S + H_E + H_{SE}, \quad (1)$$

that couples a qubit system with Hamiltonian H_S to an environment Hamiltonian H_E by the interaction H_{SE} . Without loss of generality, we assume that

$$H_{SE} = \sum_i P_i \otimes O_i, \quad (2)$$

where P_i is a string of Pauli operators acting on the system and O_i is an operator acting on the environment.

The DD problem involves designing a control Hamiltonian $H_c(t)$ acting solely on the system that suppresses the interactions with the environment. This means that after applying $H_c(t)$, the joint system–environment dynamics are governed by the decoupled Hamiltonian

$$\bar{H}_{tot} = \bar{H}_S + \bar{H}_E, \quad (3)$$

where \bar{H}_S (\bar{H}_E) denotes a (possibly) modified system (environment) Hamiltonian.

We restrict ourselves to the analysis of control Hamiltonians comprising sequences that alternate between fast single-qubit gates and free evolution intervals, where all free-evolution intervals have the same duration. These admit a natural group-theoretic description and are especially advantageous for compilation, as they simplify both the implementation and analysis of control protocols. In these cases, the effective Hamiltonian \bar{H}_{tot} can be systematically derived using tools such as Floquet theory and Magnus expansion, assuming that the expansion converges [39].

To do so, we denote the time-evolution operator generated by the control Hamiltonian $U_c(t)$ associated with $H_c(t)$ as

$$U_c(t) = \mathcal{T} \exp \left[-i \int_0^t H_c(t') dt' \right], \quad (4)$$

where \mathcal{T} is the time ordering operator and we set $\hbar = 1$. If the control Hamiltonian is cyclic with period T_c , i.e., $H_c(t) = H_c(t + T_c)$, and the initial time is at $t = 0$, the stroboscopic time evolution of the system and bath at times nT_c with $n \in \mathbb{N}$ is described by [40, 41]

$$U(nT_c) = \exp \left(-inT_c \bar{H}_{tot} \right) \quad (5)$$

where \bar{H}_{tot} is a time-independent stroboscopic Hamiltonian.

When the frequency $1/T_c$ is larger than the largest energy scale [42], the effective Hamiltonian \bar{H}_{tot} is well approximated by the first-order Magnus expansion

$$\bar{H}_{tot} \approx \frac{1}{T_c} \int_0^{T_c} U_c^\dagger(t) H_{tot} U_c(t) dt. \quad (6)$$

Higher-order corrections in the Magnus expansion can be systematically bounded using Lemma 4 of Ref. [42].

In this work, we aim to generalize this idea. Rather than focusing solely on suppressing interactions with the environment, our objective is to design DD sequences that can also selectively suppress certain interactions within the system itself. For example, we either completely freeze the system dynamics (i.e., $\bar{H}_S = 0$) or we selectively retain only some desired interactions in H_S , thereby engineering specific target Hamiltonians. This capability is particularly useful for digital-analog quantum simulations [43].

In the next section, we will briefly review the bang-bang control scheme [7, 8], which assumes instantaneous single-qubit pulses. In Appendix A, we also review the bounded-strength control scheme [35], which provides a more realistic model assuming that single-qubit gates have a finite duration. Importantly, we emphasize that the framework we introduce in this work applies to both control schemes.

B. Bang-bang control sequence

The bang-bang control scheme [7, 8] assumes that single-qubit pulses are instantaneous. The central idea is to define a decoupling group $\mathcal{G} = \{g_i\}$ [7, 24, 35], which acts on the system Hilbert space via a unitary representation $g \rightarrow U_g$. The bang-bang DD sequence is then specified by an ordered list of group elements (g_1, g_2, \dots, g_L) , with total length of the sequence $L = \lambda|\mathcal{G}|$, where $|\mathcal{G}|$ is the order of the group and λ is a positive integer, typically $\lambda = 1$ [35]. In general, each group element $g_i \in \mathcal{G}$ appears exactly λ times in the sequence. If the group \mathcal{G} is generated by a set of generators $\{\gamma_1, \dots, \gamma_n\}$, we write the group as

$$\mathcal{G} = \langle \gamma_1, \dots, \gamma_n \rangle \quad (7)$$

to explicitly denote its generating set.

A single cycle of the bang-bang control unitary $U_c(t)$ has a total duration T_c and is defined as a step function of time, divided into L equally-spaced intervals of length $\Delta = T_c/L$. During each segment, lasting for a time $\tau \in [0, \Delta)$, the control is a constant unitary operator

$$U_c[(j-1)\Delta + \tau, (j-1)\Delta] = U_{g_j}. \quad (8)$$

This control unitary is abruptly switched from $U_{g_{j-1}}$ to U_{g_j} , corresponding to an ideal instantaneous control pulse [7, 35].

Under the action of the DD group \mathcal{G} , the effective Hamiltonian \bar{H}_{tot} in Eq. (6), is given by the group twirling operation

$$\bar{H}_{tot} = \frac{1}{|\mathcal{G}|} \sum_{g \in \mathcal{G}} U_g^\dagger H_{tot} U_g := \Pi_{\mathcal{G}}(H_{tot}). \quad (9)$$

The time-evolution operator of \bar{H}_{tot} , corresponding to the time-evolution of H_{tot} at the stroboscopic times nT_c , is explicitly given by

$$U(nT_c) \approx \left(\prod_{g \in \mathcal{G}} U_g^\dagger U_\Delta U_g \right)^n, \quad (10)$$

with the free evolution operator defined as $U_\Delta = \mathcal{T} \exp \left(-i \int_0^\Delta H_{tot}(\tau) d\tau \right)$.

By Schur's lemma, the twirling channel $\Pi_{\mathcal{G}}(\cdot)$ acts as a projection and retains only the components of H_{tot} that commute with all elements of the group \mathcal{G} . When the map $g \rightarrow U_g$ defines an irreducible representation of \mathcal{G} , the projection takes the form [7, 8, 31, 35]

$$\Pi_{\mathcal{G}}(O) = \frac{\text{Tr}(O)}{d} I_d. \quad (11)$$

where d is the dimension of the system Hilbert space. In this special case, the DD sequence completely averages out all nontrivial system operators and \bar{H}_S becomes proportional to the identity. This corresponds to a trivial global phase, meaning that the system dynamics are completely frozen.

In this work, we restrict ourselves to the analysis of (π) and/or $(-\pi)$ -pulses generating X, Y, Z , and I gates on a system of N qubits. Consequently, we choose the decoupling group \mathcal{G} to be a subgroup of the N -qubit projective Pauli group, i.e. $\mathcal{G} \subseteq \mathcal{P}^N / \{\pm i, \pm 1\}$. We remark that although the Pauli group is not Abelian (i.e. $g_1 g_2 \neq g_2 g_1$), the projective Pauli group is. The corresponding unitary representation maps each group element $g \in \mathcal{G}$ to its associated standard Pauli operator acting on the system Hilbert space.

As an example, we consider one cycle of the standard single-qubit XY4 sequence, defined by the unitary time-evolution operator

$$U(T_c) = U_\Delta Y U_\Delta X U_\Delta Y U_\Delta X, \quad (12)$$

where U_Δ is a single-qubit free evolution operator for a time Δ . This sequence has a decoupling group \mathcal{G} corresponding to the full single-qubit Pauli group. This can be seen explicitly by expressing the sequence as a product of Pauli operators applied before and after each free evolution period and using Pauli matrix identities ($XY = Z$ and cyclic permutations)

$$U(T_c) \equiv (I U_\Delta I)(Y U_\Delta Y)(Z U_\Delta Z)(X U_\Delta X). \quad (13)$$

This decomposition shows that each interval is conjugated by a Pauli operator and the full sequence effectively performs a twirl over the single-qubit Pauli group. Consequently, the XY4 sequence removes all single-qubit terms, resulting in universal noise suppression.

In bounded-control schemes [32, 35], the requirement of applying arbitrarily strong and instantaneous control pulses $U_{g_{j+1}}U_{g_j}^\dagger$ at discrete times $t = j\Delta$ is relaxed. Instead, the control strategy involves smoothly interpolating between successive group elements, implementing a continuous transition from U_{g_j} to $U_{g_{j+1}}$ over each subinterval. More details on bounded-strength control scheme can be found in Appendix A.

III. PERMUTATION-INVARIANT DECOUPLING GROUP FROM HYPERGRAPH SYMMETRY

In this section, we systematically reformulate and extend the ideas introduced in Refs. [24, 27, 36] using the language of graph theory. This perspective enables a natural generalization of previous results from 2-local interaction models to general k -local interaction models. In Sec. III A, we describe the system Hamiltonian in terms of an interaction hypergraph and show that any k -local interaction induces a natural partition of physical qubits into equivalence color classes. In Sec. III, we demonstrate that this partition gives rise to a permutation symmetry that can be exploited to reduce the original interaction hypergraph to a simpler quotient hypergraph, by factoring out the symmetry group. As a result, the task of designing a DD sequence for the original interaction hypergraph is mapped to the simpler problem of designing a DD sequence for the quotient hypergraph.

A. Hypergraph coloring

To describe a general Hamiltonian of N interacting qubits, we introduce the interaction hypergraph $I_{\text{Dev}} = (V_I, E_I)$. The vertex set $V_I = \{v_1, \dots, v_N\}$ represents physical qubits. A hyperedge $e_i \in E_I$ connecting k vertices $(v_{i_1}, \dots, v_{i_k})$ corresponds to a general noise model in which arbitrary Pauli interactions from $\{I, X, Y, Z\}^{\otimes k}$ may jointly act on these k qubits, unless otherwise specified. This corresponds to the first step of Fig. 2a. A Pauli string associated with such a hyperedge is called k -local if it has support on exactly k distinct vertices. Therefore, the interaction hypergraph I_{Dev} characterizes a k -local Hamiltonian if and only if all of its hyperedges involve at most k vertices. The standard graph is simply 2-local hypergraph. Under this definition, the Hamiltonians considered in Refs. [24, 27] are 2-local and the interaction hypergraph I_{Dev} coincides with the device connectivity graph.

We now generalize the results of Refs. [24, 27] to arbitrary k -local Hamiltonians. In the first-order Magnus

expansion given in Eq. (6), a vertex v_i only interacts with other vertices that share a common hyperedge. This motivates a natural partition of the interaction hypergraph I_{Dev} . We assign a distinct color c_i to each vertex $v_i \in V_I$, such that no two vertices v_i, v_j in a hyperedge share the same color (step 2 of Fig. 2a). We denote this hypergraph coloring as $C[I_{\text{Dev}}]$, and refer to the number of colors used (i.e. the chromatic number) as χ_I .

We remark that this hypergraph coloring problem can be addressed efficiently using well-established graph-coloring algorithms [44]. However, standard graph-coloring algorithms are typically designed for graphs and not hypergraphs. To apply these algorithms to a hypergraph coloring problem, we formally construct an auxiliary graph by adding an edge between each pair of vertices v_i and v_j that share a hyperedge in I_{Dev} . A proper coloring of this auxiliary graph corresponds to a valid coloring of the original hypergraph I_{Dev} .

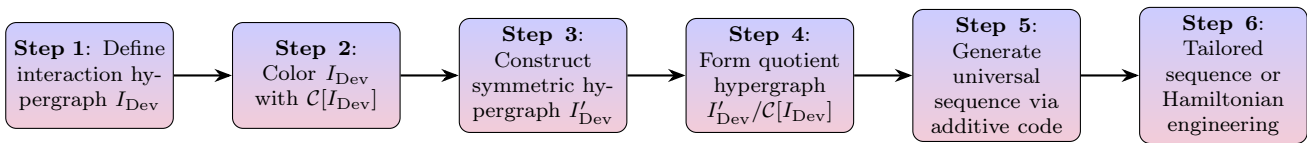
In the next section, we show that the color partition $C[I_{\text{Dev}}]$ respects an underlying hypergraph symmetry. Using this symmetry, the problem of designing a DD sequence for the interaction hypergraph I_{Dev} is significantly simplified.

B. Symmetry and quotient hypergraph

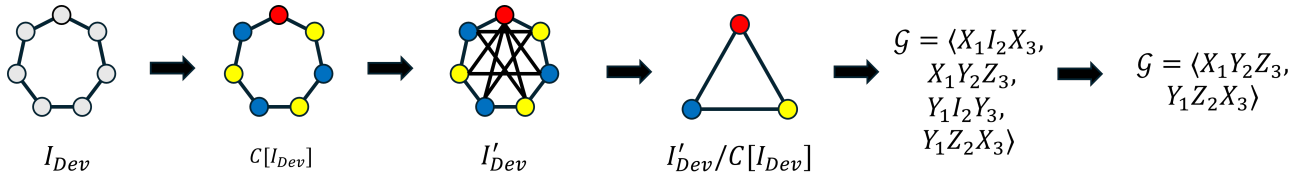
We now show how the color partition $C[I_{\text{Dev}}]$ can be exploited to simplify the problem. The strategy is as follows. We first construct an expanded hypergraph $I'_{\text{Dev}} = (V_I, E'_I)$ from I_{Dev} such that $I_{\text{Dev}} \subseteq I'_{\text{Dev}}$, and the color partition $C[I_{\text{Dev}}]$ remains a valid vertex coloring for I'_{Dev} . Because $I_{\text{Dev}} \subseteq I'_{\text{Dev}}$, any decoupling group \mathcal{G} designed for I'_{Dev} is also valid decoupling group for I_{Dev} . We then show that designing a decoupling group for I'_{Dev} is equivalent to designing one for the significantly simpler quotient hypergraph $I_{\text{Dev}}/C[I_{\text{Dev}}]$, which contains only χ_I vertices. In this way, the original problem is reduced to constructing a decoupling group for the quotient hypergraph $I'_{\text{Dev}}/C[I_{\text{Dev}}]$.

More precisely, the expanded hypergraph I'_{Dev} is constructed from I_{Dev} and its coloring $C[I_{\text{Dev}}]$ as follows. The hypergraph I'_{Dev} shares the same vertex set $V'_I = V_I$ as I_{Dev} . We traverse the colored hypergraph I_{Dev} and record all tuples $(c_{i_1}, \dots, c_{i_k})$ such that there exists a hyperedge in I_{Dev} connecting vertices with those colors. The new hyperedge set E'_I is then constructed by appending to the original set E_I additional hyperedges of the form $(v_{i_1}, \dots, v_{i_k}) \notin E_I$, where the vertices $(v_{i_1}, \dots, v_{i_k})$ have distinct colors that match one of the recorded color tuples $(c_{i_1}, \dots, c_{i_k})$. This procedure ensures that the color partition $C[I_{\text{Dev}}]$ remains valid for the hypergraph I'_{Dev} , see step 3 of Fig. 2a.

To better illustrate this construction, here we apply it to an explicit example. We consider a system of seven qubits arranged in a bilinear array with two-local interactions. Figure 3(a) illustrates the corresponding inter-



(a) Schematic overview of our decoupling framework.



(b) Example illustrating each step of the flowchart.

FIG. 2: **Framework for constructing efficient dynamical decoupling sequences.** (a) Flowchart of our approach. Starting from an interaction hypergraph, we color it, generate a symmetric variant, and construct its quotient. Additive codes are then used to produce efficient universal sequences, which are tailored to suppress specific Hamiltonian terms. (b) Example of each step in the protocol. We start from a simple 7-qubit loop (step 1) and we color it assuming a nearest-neighbor interaction model (step 2). We then construct a color-preserving symmetric hypergraph connecting all different colors (step 3), which allows us to simplify the DD problem by just considering the corresponding quotient hypergraph (step 4). The DD sequence is then constructed by using additive codes, forming a universal decoupling group that suppresses arbitrary two-local interactions (step 5). We then tailor the sequence for specific qubit architectures (step 6).

action hypergraph I_{Dev} along with its vertex coloring $C[I_{\text{Dev}}]$. A general Hamiltonian for this system is

$$H = \sum_i \vec{h}_i \cdot \vec{\sigma}_i + \sum_{\langle ij \rangle} \vec{\sigma}_i \cdot A_{ij} \vec{\sigma}_j. \quad (14)$$

where \vec{h}_i are local fields and A_{ij} are real coupling matrices that specify pairwise interactions. For this example, the expanded hypergraph I'_{Dev} constructed from the above procedure is shown in Fig. 3(b), with new edges connecting vertices of different colors.

The expanded hypergraph I'_{Dev} may appear more complex than the original interaction hypergraph I_{Dev} , suggesting that designing a suitable decoupling group \mathcal{G} for I_{Dev} could be more challenging. However, I_{Dev} inherits a strong symmetry from the color partition $C[I_{\text{Dev}}]$. In particular, I'_{Dev} is invariant under permutations of vertices that share the same color, a symmetry we (with a slight abuse of notation) also denote by $C[I_{\text{Dev}}]$. This invariance significantly simplifies the construction of the decoupling group: it implies that it suffices to consider decoupling groups \mathcal{G} that themselves respect the symmetry $C[I_{\text{Dev}}]$ [45]. Practically, this means applying identical control pulses to all qubits within the same color class.

As a complementary view on this symmetry, rather than directly working with the symmetric decoupling group \mathcal{G} , we can instead analyze the quotient hypergraph $I'_{\text{Dev}}/C[I_{\text{Dev}}]$. The quotient hypergraph $I'_{\text{Dev}}/C[I_{\text{Dev}}]$ is formed by collapsing all vertices $v_i \in V_I'$ with the same color c_i into a single super-vertex $c_i \in V_I'/C[I_{\text{Dev}}]$ in the quotient hypergraph. We will refer to the super-vertex c_i in the quotient hypergraph $I'_{\text{Dev}}/C[I_{\text{Dev}}]$ as the color class c_i . A hyperedge $(c_{i_1}, \dots, c_{i_k})$ exists in

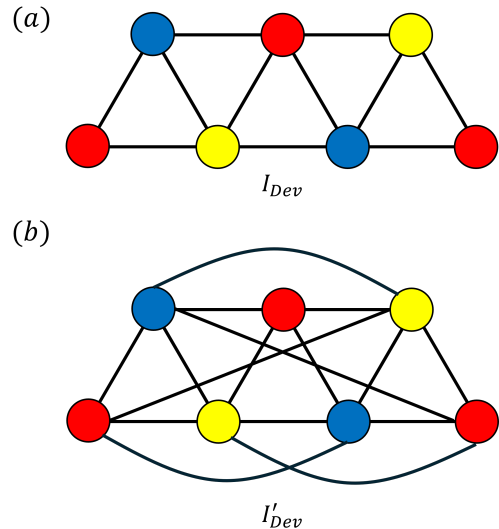


FIG. 3: **Colored bilinear array graph.** (a) Interaction hypergraph I_{Dev} of 7 physical qubits with two-local interactions arranged in a bilinear array, along with the minimal color partition $C[I_{\text{Dev}}]$. (b) Expanded hypergraph I'_{Dev} constructed from I_{Dev} and $C[I_{\text{Dev}}]$.

$I'_{\text{Dev}}/C[I_{\text{Dev}}]$ if and only if there is at least one hyperedge $(v_{i_1}, \dots, v_{i_k}) \in E_I'$, such that the vertices v_{i_j} are colored c_{i_j} respectively. Figure 4 illustrates this transformation from the expanded hypergraph I'_{Dev} (shown in Fig. 3) to its corresponding quotient hypergraph $I'_{\text{Dev}}/C[I_{\text{Dev}}]$. We emphasize that the same quotient hypergraph also captures different topologies, including the ring topology in Fig. 2.

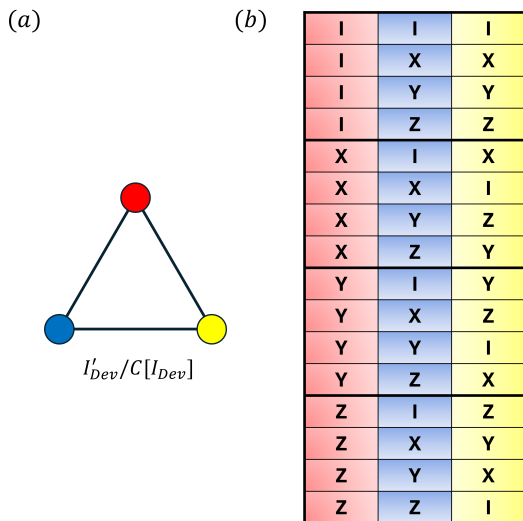


FIG. 4: **Dynamical decoupling from orthogonal arrays.** (a) The quotient hypergraph $I'_{\text{Dev}}/C[I_{\text{Dev}}]$ formed by collapsing all physical qubits of the same color in I'_{Dev} into a single equivalence class. (b) The orthogonal array $\text{OA}(L = 16, \chi_I = 3, S = 4, k = 2)$ which generates a universal DD sequence for two-local Hamiltonian defined by the quotient hypergraph $I'_{\text{Dev}}/C[I_{\text{Dev}}]$. Each column is colored according to the associated color class c_i .

It follows directly that if there is a DD sequence that universally suppresses all interactions in the quotient hypergraph $I'_{\text{Dev}}/C[I_{\text{Dev}}]$, then this sequence can be lifted to a valid decoupling sequence for the expanded hypergraph I'_{Dev} , and consequently on the interaction hypergraph I_{Dev} . The lifting procedure consists of applying the same control pulses in parallel to all vertices in I'_{Dev} that share the same color c_i . This approach is valid for both bang-bang and bounded-strength control schemes.

We note that the explicit construction of the expanded interaction hypergraph I'_{Dev} in principle is not required to design the DD group. Rather, it provides a conceptual tool that reveals the underlying symmetry structure of the colored interaction hypergraph. The expanded hypergraph also provides a key general insight, namely any two interaction hypergraphs that share the same expanded hypergraph I'_{Dev} can be universally decoupled using the same decoupling group \mathcal{G} , see the examples in Figs. 2 and 3. In fact, an even stronger statement holds: if two interaction hypergraphs share the same quotient hypergraph $I'_{\text{Dev}}/C[I_{\text{Dev}}]$ and interaction model, they admit the same decoupling group capable of universally suppressing their system interactions.

In the following section, we demonstrate how to obtain time-efficient decoupling groups for the quotient hypergraph $I'_{\text{Dev}}/C[G_{\text{Dev}}]$ using constructions from classical coding theory.

IV. TIME-EFFICIENT DECOUPLING GROUPS FROM CLASSICAL ADDITIVE CODES

In the previous section, we demonstrated how the problem of constructing a decoupling group \mathcal{G} for an arbitrary k -local interaction hypergraph I_{Dev} can be reduced to the simpler task of constructing a decoupling group for the quotient hypergraph $I'_{\text{Dev}}/C[I_{\text{Dev}}]$. In this section, we explain how to build efficient decoupling groups for $I'_{\text{Dev}}/C[I_{\text{Dev}}]$ using tools from classical coding theory. In Sec. IV A, we introduce the connection between decoupling groups \mathcal{G} and a combinatorial object known as orthogonal arrays as found in previous works [31, 32]. These objects enable constructions of decoupling groups that achieve favorable trade-offs between the DD sequence length L and the chromatic number χ_I . In Sec. IV B, we show how to construct the required orthogonal arrays from classical additive codes. In Sec. IV C, we further exploit the structure of classical additive codes to show that the decoupling group can be completely characterized by its generators, thereby reducing the design of the full decoupling group to the simpler task of designing its generators. Finally, in Sec. IV D, we present a simple numerical algorithm for finding decoupling groups that selectively cancel certain interactions while preserving others.

A. Orthogonal arrays and dynamical decoupling

Time-efficient DD sequences can be constructed using combinatorial design objects. For example, Ref. [27] employs Hadamard matrices to construct decoupling sequences for 2-local Hamiltonians. We generalize this approach to arbitrary k -local Hamiltonians by using more general combinatorial structures known as orthogonal arrays [31, 32, 46]. In the following analysis, we consider the worst-case scenario where all possible k -local interactions between the color classes c_i are present in the quotient hypergraph $I'_{\text{Dev}}/C[I_{\text{Dev}}]$.

An orthogonal array $\text{OA}(L, \chi_I, S, k)$ is an $L \times \chi_I$ array with entries taken from a finite set S and strength k , such that every possible k -tuple from $S^{\otimes k}$ appears uniformly across any choice of k columns [47]. In this work, we restrict ourselves to the set $S = \{I, X, Y, Z\}$ of single-qubit Pauli operators. Each column of the orthogonal array is associated with a color class c_i , and each row defines a group element in the decoupling group \mathcal{G} . If the noise model is biased along a specific axis of the Bloch sphere (e.g. the Z -axis) or if we want to maintain certain interactions (e.g. XX interactions), we can reduce the required size L of the orthogonal array by selecting a smaller set (e.g. $S = \{I, X\}$) instead of the full single-qubit Pauli group. We remark that for any choice of parameters χ_I , S , and strength k , there always exists an orthogonal array whose length L is determined by these parameters [47].

In Fig. 4, we show the explicit orthogonal array

OA($L = 16, \chi_I = 3, |S| = 4, k = 2$), which generates a universal decoupling sequence for 2-local Hamiltonians defined on the quotient hypergraph $I'_{\text{Dev}}/C[I_{\text{Dev}}]$ [48]. One can verify that for any pair of columns, the rows of the OA exhaustively span all combinations of $\{I, X, Y, Z\}^{\otimes 2}$ exactly once. Moreover, each Pauli operator appears exactly four times in every column, ensuring balanced coverage and uniformity.

By construction, the action of the decoupling group \mathcal{G} derived from an OA with strength k implements a group twirl over the k -fold Pauli group $\{I, X, Y, Z\}^{\otimes k}$ on any subset of k color classes. As a consequence, all k -local interaction terms are dynamically suppressed, following directly from Schur's lemma [Eq. (11)]. Furthermore, all interactions with support on less than k color classes are also suppressed as a consequence of this construction. Therefore, to universally decouple all k -local interactions on the quotient hypergraph $I'_{\text{Dev}}/C[I_{\text{Dev}}]$, it suffices to construct the orthogonal array OA(L, χ_I, S, k).

We note that there is a comprehensive online library cataloging efficient (i.e good ratio between χ_I and L) orthogonal arrays across a wide range of parameters [48]. In the next section, we describe how to construct length-efficient orthogonal arrays by utilizing their connection to classical error correction codes [31, 32]. Since classical codes are extensively studied, we can utilize well-established classical codes to obtain time-efficient DD sequences suppressing arbitrary k -local interactions [32].

B. Orthogonal array and classical additive codes

The connection between orthogonal arrays and classical linear codes is well established [31, 32, 47, 49]. In this work, we focus on the projective Pauli group, which admits a natural isomorphism to the finite field \mathbb{F}_4 . A finite field \mathbb{F}_q is a set containing q elements in which addition, subtraction, multiplication, and division (except by zero) are all well-defined and satisfy the field axioms. The isomorphism between the projective Pauli group and \mathbb{F}_4 is defined by the correspondence

$$I \rightarrow 0, X \rightarrow 1, Z \rightarrow \omega, Y \rightarrow 1 + \omega, \quad (15)$$

where ω is a primitive element of \mathbb{F}_4 satisfying $\omega^2 = \omega + 1$. The addition and multiplication tables for \mathbb{F}_4 are

$$\begin{array}{c|cccc} + & 0 & 1 & \omega & 1 + \omega \\ \hline 0 & 0 & 1 & \omega & 1 + \omega \\ 1 & 1 & 0 & 1 + \omega & \omega \\ \omega & \omega & 1 + \omega & 0 & 1 \\ 1 + \omega & 1 + \omega & \omega & 1 & 0 \end{array} \quad (16)$$

and

$$\begin{array}{c|cccc} \times & 0 & 1 & \omega & 1 + \omega \\ \hline 0 & 0 & 0 & 0 & 0 \\ 1 & 0 & 1 & \omega & 1 + \omega \\ \omega & 0 & \omega & 1 + \omega & 1 \\ 1 + \omega & 0 & 1 + \omega & 1 & \omega \end{array} . \quad (17)$$

This correspondence allows us to represent Pauli operators algebraically as elements of \mathbb{F}_4 , providing a convenient framework for constructing orthogonal arrays from quaternary codes. Furthermore, when the noise is biased (e.g. along the Z -axis), we may restrict to a subset of the Pauli group, in which case classical codes over the binary field \mathbb{F}_2 become relevant.

We consider here classical additive codes, which, as we will show in Sec. IV C, provide a natural framework for interpreting a decoupling sequence as an error detection code. An additive code \mathcal{C} is a subset of \mathbb{F}_q^n (a vector of length n in which its entries are from \mathbb{F}_q) that is closed under addition. While every linear code is an additive code, the converse is not true: additive codes are not necessarily closed under scalar multiplication unless the field is \mathbb{F}_2 .

We characterize the code \mathcal{C} by the set of parameters $(n, |\mathcal{C}|, d)_q$, where n is the length of the codeword, $|\mathcal{C}|$ is the number of distinct code words, and d is the code distance. The entries of each codeword are elements of the finite field \mathbb{F}_q . The distance d is defined as the minimum Hamming distance between any two distinct codewords $\mathbf{u}, \mathbf{v} \in \mathcal{C}$. Since \mathcal{C} is closed under addition, this is equivalent to the minimum Hamming weight of any nonzero codeword

$$d = \min_{\mathbf{u} \neq \mathbf{0} \in \mathcal{C}} \text{wt}_{\text{H}}(\mathbf{u}). \quad (18)$$

The vector space \mathbb{F}_4^n can be endowed with an inner product $\langle \cdot, \cdot \rangle$. A natural choice for additive codes is the trace Hermitian inner product $\langle \cdot, \cdot \rangle_{\text{tr}} : \mathbb{F}_4^n \rightarrow \mathbb{F}_2$ [50], defined as

$$\langle \mathbf{u}, \mathbf{v} \rangle_{\text{tr}} = \sum_{\mathbf{i}} (\mathbf{u}_{\mathbf{i}} \mathbf{v}_{\mathbf{i}}^2 + \mathbf{v}_{\mathbf{i}} \mathbf{u}_{\mathbf{i}}^2). \quad (19)$$

Under the mapping between single-qubit Pauli operators and elements of \mathbb{F}_4 given in Eq. (15), this inner product directly gives the commutation relations of Pauli operators. That is, it evaluates to zero if the corresponding Pauli operators commute and to one if they anticommute.

Using the trace Hermitian inner product, we define the dual code \mathcal{C}^\perp of an additive code \mathcal{C} as

$$\mathcal{C}^\perp = \{\mathbf{v} \in \mathbb{F}_4^n \mid \langle \mathbf{u}, \mathbf{v} \rangle_{\text{tr}} = \mathbf{0}, \quad \forall \mathbf{u} \in \mathcal{C}\}. \quad (20)$$

We denote the minimum distance of the dual code by d^\perp . Importantly, the dual code \mathcal{C}^\perp is always an additive code, regardless of whether \mathcal{C} is linear or additive. However, it is known that if \mathcal{C} is an additive code of size $|\mathcal{C}| = 2^l$ for some positive integer $l \leq 2n$, then its dual code has size $|\mathcal{C}^\perp| = 2^{2n-l}$. This follows from the fact that \mathbb{F}_4^n is isomorphic to \mathbb{F}_2^{2n} under addition.

A seminal result by Delsarte [49] establishes a fundamental connection between orthogonal arrays and classical codes:

Theorem IV.1. *If \mathcal{C} is a code $(n, |\mathcal{C}|, d)_q$ with dual distance d^\perp , then the codewords of \mathcal{C} form the rows of an*

$OA(|\mathcal{C}|, n, q, d^\perp - 1)$ with entries from \mathbb{F}_q . Conversely, the rows of a linear $OA(|\mathcal{C}|, n, q, k)$ over \mathbb{F}_q form a linear code $(n, |\mathcal{C}|, d)_q$ over \mathbb{F}_q with dual distance $d^\perp \geq k + 1$. If the orthogonal array has strength k but not $k + 1$, d^\perp is precisely $k + 1$.

This theorem highlights the direct connection between the strength of an OA and the dual distance d^\perp of the code \mathcal{C} . Consequently, to construct an OA of strength k , corresponding to a universal DD sequence that suppresses k -local interactions in the original Hamiltonian, it suffices to use the dual code \mathcal{C}^\perp of a code \mathcal{C} with distance $d = k + 1$.

In Ref. [32], Bose–Chaudhuri–Hocquenghem (BCH) codes [51, 52] were used to construct efficient universal DD sequences for k -local Hamiltonians acting on physical qubits, not color classes. By applying their construction to the quotient hypergraph $I_{\text{Dev}}/C[I_{\text{Dev}}]$, we find that the length L of a single DD cycle required to universally decouple k -local Hamiltonians scales as

$$O(\chi_I^{k-1}) \quad (21)$$

for bang-bang control, and as

$$O(\chi_I^{k-1} \log \chi_I) \quad (22)$$

for bounded-strength control (see Appendix A).

In Sec. V, we will present different constructions based on alternative classical codes that generate more time-efficient decoupling groups for 2-local and 3-local Hamiltonians. While the asymptotic scaling remains the same as in Eqs. (21) and (22), our constructions lead to improved constant prefactors compared to those based on BCH codes for the 2-local and 3-local Hamiltonians.

C. Dynamical decoupling as error detection codes

Historically, self-dual additive codes over \mathbb{F}_4 (i.e., $\mathcal{C} = \mathcal{C}^\perp$) have played a central role in the construction of stabilizer quantum error-correcting codes [50, 53–55]. Many properties of stabilizer codes can be analyzed through their stabilizer generators. In a closely analogous manner, we further develop the connection between dynamical decoupling and classical additive codes by showing that key properties of a DD sequence can be analyzed through the generators of its decoupling group. This perspective not only provides a compact characterization of DD sequences, but also enables systematic constructions of selective DD sequences, as we explain in this section.

From the definition of the dual code \mathcal{C}^\perp in Eq. (20), it follows that Pauli strings corresponding to codewords in \mathcal{C}^\perp remain invariant under the decoupling sequence generated by \mathcal{C} . In fact, \mathcal{C}^\perp defines the entire invariant subspace of the decoupling sequence. Consequently, to determine whether an interaction is suppressed by the decoupling sequence, one only needs to check whether the associated codeword lies in \mathcal{C}^\perp . At first glance, this

may appear computationally expensive because it requires checking the trace Hermitian inner product against all codewords in \mathcal{C} . However, it is not necessary to check the entire code. Instead, it is sufficient to compute the inner products with respect to the generators of \mathcal{C} , which fully characterize the code.

Because \mathcal{C} is an additive code, it is generated by a finite set of independent generators $\Gamma = \{\gamma_1, \dots, \gamma_m\}$, where $|\Gamma| = \log_2 |\mathcal{C}|$. Importantly, if a vector $\mathbf{u} \in \mathbb{F}_4^n$ anticommutes with at least one of the generators γ_i , then the Pauli string associated with \mathbf{u} will be suppressed by the decoupling sequence generated from the code \mathcal{C} [21].

This can be seen explicitly through a simple example. Suppose \mathcal{C} , and equivalently the decoupling group \mathcal{G} , has two generators γ_1 and γ_2 . The decoupling group is then given by

$$\mathcal{G} = \{I, \gamma_1, \gamma_2, \gamma_1\gamma_2\}. \quad (23)$$

We assume without loss of generality that \mathbf{u} anticommutes with γ_1 but commutes with γ_2 . Under conjugation by the elements of \mathcal{G} , the sign of the Pauli string corresponding to \mathbf{u} evolves as

$$\{+1, -1, +1, -1\}. \quad (24)$$

When twirling over the group \mathcal{G} , all these contributions cancel out, and the corresponding interaction is completely suppressed by the decoupling sequence. The generalization to an arbitrary set of generators Γ follows directly from the same principle: if \mathbf{u} anticommutes with any generator in Γ , then averaging over the decoupling group results in the complete cancellation of the corresponding Pauli term.

We have shown that DD sequences constructed from classical additive codes behave analogously to quantum stabilizer codes. However, we emphasize two key differences. First, unlike quantum stabilizer codes, we do not require the generators of the decoupling group \mathcal{G} to commute with each other. Second, in the context of dynamical decoupling, there is no active "correction" step. Instead, the twirling procedure passively removes all components of the Hamiltonian that anticommute with at least one of the generators of \mathcal{G} . In this sense, the role of the decoupling sequence is similar to that of an *error detection code* rather than an error correction code.

The connection between designing decoupling sequences and designing error detection codes is a key insight of our work. Specifically, if the dominant residual interactions in the system are known, we can forego a universal decoupling group \mathcal{G} , which suppresses all interactions, and instead remove certain generators from \mathcal{G} while still suppressing the dominant residual terms [20]. The resulting DD sequence length becomes significantly shorter. We will make extensive use of this idea in Sec. VA and VB, where we tailor our general method to specific cases.

As an example, the orthogonal array presented in Fig. 4 that universally decouples all 2-local interactions

is generated by the decoupling group

$$\mathcal{G} = \langle X_1 I_2 X_3, X_1 Y_2 Z_3, Y_1 I_2 Y_3, Y_1 Z_2 X_3 \rangle \quad (25)$$

However, if we know that the residual two-qubit interactions are restricted to terms of the form $X_i X_j, Y_i Y_j$, or $Z_i Z_j$, as in spin qubits [56–59], the reduced decoupling group

$$\mathcal{G}_{\text{red}} = \langle X_1 Y_2 Z_3, Y_1 Z_2 X_3 \rangle \quad (26)$$

still suppress all the relevant residual interactions. Explicitly, the elements of \mathcal{G}_{red} are

$$\mathcal{G}_{\text{red}} = \{I_1 I_2 I_3, X_1 Y_2 Z_3, Y_1 Z_2 X_3, Z_1 X_2 Y_3\}. \quad (27)$$

We note that this group corresponds to running the standard XY4 sequence in parallel on all three qubits, with the XY4 cycles on the second and third qubits being cyclically shifted relative to each other. Moreover, the reduced group \mathcal{G}_{red} still universally decouples all single-qubit terms. As a result, the DD sequence requires only $2^2 = 4$ time steps instead of $2^4 = 16$, achieving a fourfold reduction in cycle length.

Another interesting consequence of our error-detection perspective is that it enables the construction of decoupling sequences that selectively suppress certain interactions while preserving others [24, 60]. For instance, in systems where anisotropic exchange interactions arise, such as spin qubits with strong spin-orbit coupling [60–62], the decoupling sequence generated by Eq. (26) preserves specific components of the antisymmetric Dzyaloshinskii–Moriya (DM) interaction. In particular, it maintains terms of the form:

$$\{X_1 Y_2, Y_1 Z_2, Y_2 Z_3, Z_2 X_3, X_1 Z_3, Y_1 X_3\}. \quad (28)$$

By alternating between DD sequences derived from \mathcal{G}_{red} and suitably permuted variants of it, one can fully preserve the complete DM interaction, thus enabling new possibilities for quantum simulation [63, 64].

We will discuss more examples of sequences simulating certain Hamiltonians in Sec. V C. In the next section, we introduce a simple search algorithm to construct selective DD sequences.

Finally, we remark that if one uses a quantum stabilizer code (i.e a self-dual additive code) to construct a DD sequence in parallel with employing the same code for active quantum error correction, it is possible to improve the overall quantum code performance by suppressing high-weight errors. This idea was explored in Refs. [20, 21], where the authors designed decoupling sequences based on the stabilizers and logical operators of a quantum code to suppress high-weight error strings. We do not directly compare our sequences with those proposed in Refs. [20, 21], as they serve fundamentally different purposes. The sequences in their work scale exponentially with the quantum code (system) size but are used alongside a quantum error-correcting code, such that errors that accumulate due to the long sequence length

can be actively corrected. In contrast, our sequences are designed to protect bare physical qubits without additional quantum error correction. An interesting direction for future work is combining our approach with that of Refs. [20, 21], to explore trade-offs between sequence length and robustness against errors in the presence of a quantum stabilizer code.

D. Selective DD sequences

We now apply our formalism to selectively suppress only particular interactions, rather than to completely decouple the system from the environment or freeze the system dynamic. To do so, we assume that the system Hamiltonian H_S can be decomposed into two parts:

$$H_S = H_S^{\parallel} + H_S^{\perp}, \quad (29)$$

where H_S^{\parallel} contains the interaction terms we wish to preserve and H_S^{\perp} contains the terms we aim to suppress. This task is particularly relevant for applications such as Hamiltonian simulation, where it is desirable to selectively engineer specific interactions [30].

Based on the connection between DD sequences and error-detection codes, we can construct a simple algorithm that finds the decoupling group performing this task. Our method explicitly searches for generators of the DD group that suppresses the undesired terms in H_S^{\perp} while preserving the desired terms in H_S^{\parallel} .

As a first step, we identify a set of generators that commute with all terms in H_S^{\parallel} . This is efficiently achieved by representing each Pauli string in H_S^{\parallel} as a binary vector in \mathbb{F}_2^{2n} via the symplectic representation

$$P = \left(\prod_{i=1}^n X_i^{x_i} Z_i^{z_i} \right) \rightarrow (\vec{x} \mid \vec{z})^T \quad \text{with } \vec{x}, \vec{z} \in \mathbb{F}_2^n. \quad (30)$$

In the symplectic representation, the commutation relation between two Pauli strings \mathbf{u} and \mathbf{v} is determined by their symplectic inner product

$$\mathbf{u}^T \Omega \mathbf{v}, \quad \text{where } \Omega = \begin{pmatrix} 0_{n \times n} & I_{n \times n} \\ I_{n \times n} & 0_{n \times n} \end{pmatrix}. \quad (31)$$

The two strings commute if and only if this inner product is zero.

Let $\{\mathbf{h}_i\}_{i=1}^M$ be the binary vector representations of the Pauli strings in H_S^{\parallel} , where M is the number of strings. The set of binary vectors (and corresponding Pauli strings) that commute with all elements of H_S^{\parallel} forms the null space of the matrix

$$\begin{pmatrix} (\mathbf{h}_1^{\parallel})^T \\ \vdots \\ (\mathbf{h}_M^{\parallel})^T \end{pmatrix} \Omega. \quad (32)$$

This null space can be efficiently computed via standard Gaussian elimination over \mathbb{F}_2 .

Let $\{\mathbf{n}_i\}$ denote the binary vector generators of the null space from Eq. (32). To construct a minimal decoupling sequence that suppresses H_S^\perp , we form a bipartite graph whose two partitions consist of the null space generators $\{\mathbf{n}_i\}$ and the Pauli terms $\{\mathbf{h}_i^\perp\}$ from H_S^\perp . An edge is drawn between \mathbf{n}_i and \mathbf{h}_j^\perp if and only if they anti-commute, i.e.

$$\mathbf{n}_i^T \Omega \mathbf{h}_j^\perp = 1 \pmod{2}. \quad (33)$$

Constructing this graph requires computing all pairwise symplectic inner products, with a total complexity of $O(|\{\mathbf{n}_i\}||\{\mathbf{h}_i^\perp\}|)$.

Given the bipartite graph, we numerically identify the minimal set of generators $\{\mathbf{n}_i\}$ that preserves H_S^\parallel while decoupling H_S^\perp . This reduces to the classical minimum set cover problem: finding the smallest subset of $\{\mathbf{n}_i\}$ such that every \mathbf{h}_i^\perp anticommutes with at least one selected generator. While the minimum set cover is generally a NP-hard problem, this problem remains tractable in simple cases, where we assume the chromatic number χ_I is small, an assumption typically valid for planar devices with short range interactions. We remark that a minimum covering set does not always exist (i.e., some terms in H_S^\perp may be product of terms in H_S^\parallel). In such cases, one can instead employ the integer programming method introduced in Ref. [30].

We emphasize that this algorithm is primarily a proof of concept rather than a fully optimized solution. Nonetheless, it shows that the error-detection perspective can drastically reduce the search space by focusing only on the generators of the decoupling group instead of the entire sequence, generally enabling a more efficient and automated construction of tailored decoupling sequences. This viewpoint could also potentially benefit machine learning-based approaches [36, 37] to designing robust DD sequences.

V. APPLICATIONS TO QUANTUM COMPUTING

In the previous sections, we explained how to construct time-efficient DD sequences for arbitrary k -local Hamiltonians using tools from classical coding theory. In this section, we present concrete applications of our framework based on well-known families of classical codes. We postpone the discussion of sequence robustness against pulse imperfections to Sec. VI. In Sec. VA, we show how to construct DD sequences tailored to superconducting qubit architectures using Reed–Muller codes. In Sec. VB, we develop DD sequences that suppress general two- and three-local errors using projective geometry codes, and demonstrate how to adapt these constructions to spin-qubit platforms. Finally, in Sec. VC, we show how our framework can be used to simulate Ki-

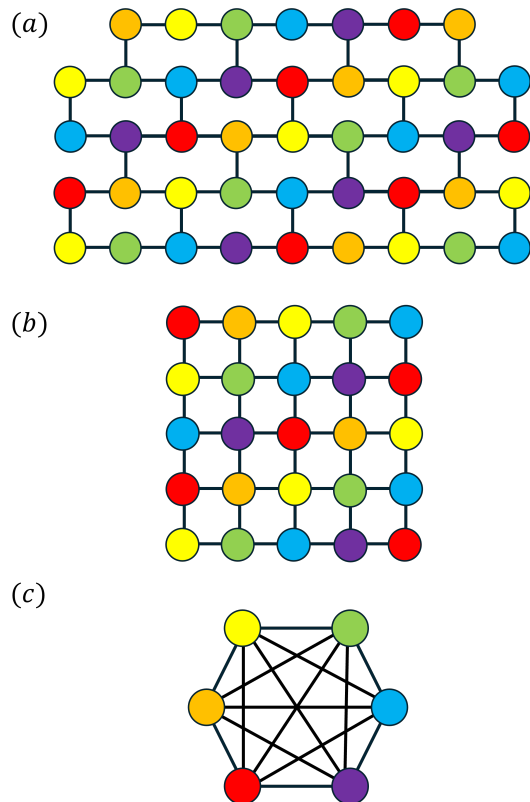


FIG. 5: **Colored graphs of common superconducting qubit architectures.** We assume a noise model where each qubit experiences both longitudinal coherence errors (X and Y errors), along with residual ZZ interactions between nearest- and next-nearest-neighbors, and ZZZ interactions among any three consecutive qubits. The colorings also apply when residual ZZ interactions extend to next-nearest neighbors. (a) Heavy-hex lattice with $\chi_I = 6$ colors. (b) Square lattice with $\chi_I = 6$ colors. (c) The resulting quotient hypergraph is identical for both architectures.

taev’s honeycomb model starting from the isotropic exchange Hamiltonian native to spin-qubit platforms.

A. Residual ZZ and ZZZ coupling in superconducting qubits

1. Suppressing ZZZ coupling

In superconducting platforms, suppressing residual ZZ and ZZZ couplings between neighboring qubits is a key challenge for scalability, as these interactions are a major source of coherent errors [65–67]. In this section, we show that by combining the hypergraph coloring procedure introduced earlier with binary Reed–Muller codes, one can construct efficient DD sequences tailored to superconducting qubits. Specifically, we introduce a bang-bang control sequence with length scaling as $O(\chi_I)$. In

Appendix B, we extend this result to bounded-strength control, yielding a DD sequence with length scaling as $O(\chi_I \log \chi_I)$.

As a concrete example, Fig. 5(a) and Fig. 5(b) show the color partitions using $\chi_I = 6$ for the heavy-hex lattice and the square lattice, used by IBM [68] and Google [69] respectively. In this section, we assume a noise model in which each qubit is subject to both longitudinal and transversal coherence errors, along with residual ZZ interactions between neighboring qubits and ZZZ interactions across any three consecutive qubits. The presented color partitions also apply when considering residual ZZ interactions between both nearest and next-nearest neighbors. Fig. 5(c) shows the corresponding quotient hypergraph induced by the color partition. We emphasize that both the heavy-hex and square lattices yield the same quotient hypergraph under this partitioning. In the following, we briefly review the Reed–Muller code and outline how to construct tailored DD sequences for superconducting qubits based on it.

The Reed-Muller code is one of the oldest and simplest families of linear binary codes with well-understood parameters and dual structure [70]. A Reed-Muller code $\text{RM}(r, m)$ is a binary code with parameters

$$(n, |\mathcal{C}|, d)_q = (2^m, 2^{\sum_{i=0}^r \binom{m}{i}}, 2^{m-r})_2 \quad (34)$$

The dual of $\text{RM}(r, m)$ is also a Reed-Muller code, specifically $\text{RM}(m-r-1, m)$. The generators $\{\gamma_i\}$ of the Reed-Muller code $\text{RM}(r, m)$ can be constructed using Boolean polynomials of degree at most r . Each generator γ_i corresponds to a monomial of the form

$$\gamma_i \rightarrow f_{\gamma_i}(\mathbf{x}) = x_{i_1} x_{i_2} \dots x_{i_s}, \quad (35)$$

where $\mathbf{x} = (x_1, \dots, x_m) \in \mathbb{F}_2^m$, $0 \leq s \leq r$, and the total degree of f_{γ_i} is at most r . There are exactly

$$\sum_{i=0}^r \binom{m}{i} \quad (36)$$

linearly independent monomials, corresponding to the dimension of the code. Each generator γ_i is a binary vector of length 2^m obtained by evaluating the associated polynomial $f_{\gamma_i}(\mathbf{x})$ at all 2^m possible bit strings $\mathbf{x} \in \mathbb{F}_2^m$.

We will use the Reed-Muller code $\mathcal{C} = \text{RM}(1, m)$ to construct our DD sequence. The dual code of $\text{RM}(1, m)$ is $\mathcal{C}^\perp = \text{RM}(m-2, m)$, consequently, it has the dual distance

$$d^\perp = 2^{m-(m-2)} = 4. \quad (37)$$

If we replace each codeword in \mathcal{C} by substituting 0 with the identity I and 1 with X , then Theorem IV.1 ensures that the resulting DD sequence suppresses all Z -type interactions with weight up to $d^\perp - 1 = 3$.

The generators of $\text{RM}(1, m)$ correspond to all linear Boolean functions over \mathbb{F}_2^m , i.e., the constant function $f_{\gamma_0} = 1$ and the monomials $f_{\gamma_i} = x_i$ with $i = 1, \dots, m$.

As an example, Table Ia lists the generators of $\text{RM}(1, 3)$ as rows, corresponding to the chromatic number $\chi_I = 2^3 = 8$. The generator γ_0 (first row) associated with the constant function $f_{\gamma_0} = 1$ can suppress all single-qubit Z_i terms as well as any three-qubit $Z_i Z_j Z_k$ terms. In addition, the other generators $\gamma_{i \geq 1}$ suppress two-qubit $Z_i Z_j$ interactions between qubits with distinct colors. Importantly, since the heavy-hex and square lattices in Fig. 5 require only $\chi_I = 6$ colors, the DD sequence derived from Table Ia is directly applicable to these architectures.

C_1	C_2	C_3	C_4	C_5	C_6	C_7	C_8
1	1	1	1	1	1	1	1
1	1	1	1	0	0	0	0
1	1	0	0	1	1	0	0
1	0	1	0	1	0	1	0

(a) Binary generator matrix of $\text{RM}(1, 3)$.

C_1	C_2	C_3	C_4	C_5	C_6	C_7	C_8
X	X	X	X	X	X	X	X
X	X	X	X	Z	Z	Z	Z
X	X	I	I	X	X	I	I
Y	Z	Y	Z	Y	Z	Y	Z

(b) Universal modified generator with Pauli substitutions.

C_1	C_2	C_3	C_4	C_5	C_6	C_7
X	X	X	X	Z	Z	Z
X	X	I	I	X	X	I
Y	Z	Y	Z	Y	Z	Y

(c) Punctured universal modified generator after removing C_8 .

TABLE I: Suppressing ZZ and ZZZ interactions. Summary of the generator matrices based on the Reed-Muller $\text{RM}(1, 3)$ code. (a) Binary generator. (b) Universal modified generator with Pauli substitutions for universal decoupling. (c) Punctured version optimized for two-body interactions with one fewer color.

The DD sequence constructed from the $\text{RM}(1, m)$ code using the mapping $0 \rightarrow I$ and $1 \rightarrow X$ can only suppress Z -type interactions. However, to universally suppress all single-qubit terms in addition to residual $Z_i Z_j$ and $Z_i Z_j Z_k$ couplings, a simple modification suffices. The key idea is that the mapping can be generalized by assigning "0" to I or Z , and "1" to either X or Y . The resulting decoupling sequence still removes all Z -type interactions of weight up to three.

To universally decouple single-qubit terms, we require that the support of the generators on each color class must include at least two distinct Pauli operators from $\{X, Y, Z\}$. In other words, each column in Table Ia must contain at least two different Pauli matrices. This condition can always be satisfied for the generators of $\text{RM}(1, m)$ by appropriately applying the substitution rule discussed above. Table Ib provides an example of the modified substitution applied to Table Ia. Consequently, the length L of the decoupling sequence constructed

based on the Reed-Muller codes is given by

$$L = 2^{\lceil \log_2(\chi_I) \rceil + 1} \sim O(\chi_I). \quad (38)$$

In practical terms, this means that for the near-term architectures shown in Fig. 5, a tailored bang-bang decoupling sequence of length $L = 16$ is sufficient to protect superconducting qubit systems against 3-local interactions. In contrast, as we will show later, using a universal DD sequence that suppresses all 3-local interactions requires a significantly longer sequence of length $L = 64$, a fourfold increase.

2. Tailored sequence to only ZZ couplings

Our DD sequence based on Reed-Muller codes can universally suppress single-qubit terms, as well as two-qubit $Z_i Z_j$ and three-qubit $Z_i Z_j Z_k$ interactions. However, if three-qubit interactions are negligible or absent, we can further improve the length of the sequence. The improvement originates from two factors. First, restricting to two-body interactions reduces the chromatic number χ_I of the interaction hypergraph. Second, we can drop one generator from the $\text{RM}(1, m)$ code, effectively halving the length of the decoupling sequence.

The generator we remove is γ_0 which, as previously discussed, suppresses all weight-three Z -type terms. As a consequence, the final color class C_{2^m} (corresponding to the last column of Table Ib) can no longer suppress single-qubit Z terms. Therefore, we must also remove this color class. Removing color class C_{2^m} is equivalent to constructing a punctured Reed-Muller code. However, since we also discard γ_0 generator, the resulting code is a modified punctured $\text{RM}(1, m)$ code with dual distance $d^\perp = 3$ instead of $d^\perp = 4$. Consequently, the length of the DD sequence is

$$L = 2^{\lceil \log_2(\chi_I + 1) \rceil} \sim O(\chi_I). \quad (39)$$

The resulting decoupling sequence universally suppresses single-qubit terms and two-qubit $Z_i Z_j$ interactions, while requiring one fewer generator at the cost of one fewer color. In Table Ic, we present the generators of the decoupling sequence generated from Table Ib by removing the first row and the last column. This modified punctured $\text{RM}(1, m)$ construction is, up to minor adjustments, equivalent to the single-axis Hadamard construction introduced in Ref. [27].

This means that to protect superconducting qubit systems with the architecture shown in Fig. 5 against both nearest-neighbor and next-nearest-neighbor ZZ couplings, a tailored bang-bang DD sequence of length $L = 8$ suffices. In contrast, as we will show later, a universal DD sequence that suppresses all interactions up to the same range requires a significantly longer sequence of length $L = 32$, again a fourfold increase.

In this section, we have shown how to construct tailored bang-bang DD sequences for suppressing residual

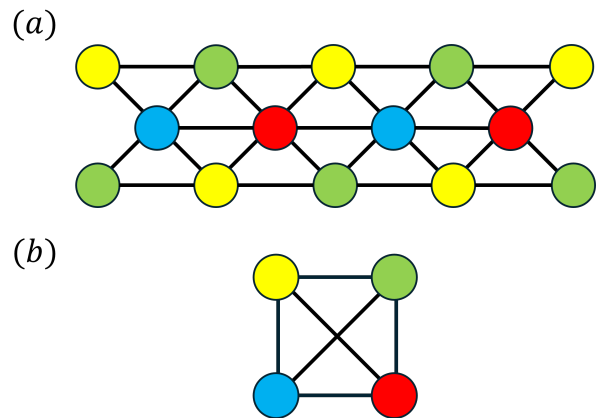


FIG. 6: **Colored trilinear array architecture in the spin-qubit platform.** We assume a noise model where each qubit undergoes both longitudinal and transversal coherent error, with Heisenberg exchange between neighbors and scalar chirality interactions among any three qubits forming a triangle. (a) The color partition $C[I_{\text{Dev}}]$ uses $\chi_I = 4$ colors, tailored to this interaction model. (b) The resulting quotient hypergraph is a square with diagonal links.

interactions in superconducting qubits by using binary Reed-Muller codes. In Appendix B, we extend this construction to bounded-strength control sequences. In the next section, we turn to the spin-qubit platform and introduce tailored decoupling sequences based on quaternary codes.

B. Exchange interactions in spin qubits

Dense spin-qubit architectures are challenged by residual exchange interaction [60, 61, 71] that cannot be completely turned off. The dominant residual interactions for spin-qubit systems with small spin-orbit interaction are the two-qubit Heisenberg exchange interactions

$$\sigma_i \cdot \sigma_j, \quad (40)$$

and the scalar chirality interaction [72] (for perpendicular magnetic fields)

$$\sigma_i \cdot (\sigma_j \times \sigma_k). \quad (41)$$

The class of three-local Hamiltonians is particularly important, as it enables the implementation of single-step, high-fidelity three-qubit gates [60, 73, 74]. As a concrete example, we consider a trilinear array architecture [75] designed to support such gates, as illustrated in Fig. 6(a) [60]. We assume a noise model in which each qubit experiences both longitudinal and transversal coherent error, along with Heisenberg exchange interactions between neighboring qubits and scalar chirality interactions among any trio forming a triangle. Under this interaction model, the array admits a color partition

C_1	C_2	C_3	C_4	C_5
1 0	0 0	1 0	1 0	1 0
0 1	0 0	1 1	0 1	1 1
0 0	1 0	0 1	1 0	1 1
0 0	0 1	1 0	0 1	0 1

C_1	C_2	C_3	C_4	C_5
1	0	1	1	1
ω	0	$1 + \omega$	ω	$1 + \omega$
0	1	ω	1	$1 + \omega$
0	ω	1	ω	ω

C_1	C_2	C_3	C_4	C_5
X	I	X	X	X
Z	I	Y	Z	Y
I	X	Z	X	Y
I	Z	X	Z	Z

(a)

C_1	C_2	C_3	C_4	C_5	C_6	C_7	C_8	C_9	C_{10}	C_{11}	C_{12}	C_{13}	C_{14}	C_{15}
X	Z	Y	I	I	I	X	Z	Y	X	Z	Y	X	Z	Y
Z	Y	X	I	I	I	Y	X	Z	Z	Y	X	Y	X	Z
I	I	I	X	Z	Y	Z	Y	X	X	Z	Y	Y	X	Z
I	I	I	Z	Y	X	X	Z	Y	Z	Y	X	Z	Y	X

(b)

TABLE II: **Universal suppression of two-local and Heisenberg exchange interactions.** These tables illustrate how to derive DD groups from additive projective geometry codes based on a 1-spread in $\text{PG}(3, 2)$. (a) Left: A (complete) 1-spread in $\text{PG}(3, 2)$, where each column represents a line described by two projective points in \mathbb{F}_2^4 . Center: The corresponding projective points in $\text{PG}(3, 4)$ constructed from the 1-spread in $\text{PG}(3, 2)$ using Eq. (49). Right: The additive generators of a DD group that universally suppress two-local interactions constructed from projective points in $\text{PG}(3, 4)$. (b) Generators of DD group tailored for spin-qubit systems based on a 1-spread in $\text{PG}(3, 2)$. Each projective point in $\text{PG}(3, 4)$ is expanded into its three equivalent representatives in \mathbb{F}_4^4 , tripling the number of color classes.

with $\chi_I = 4$ colors. The resulting quotient hypergraph is shown in Fig. 6(b).

To construct a tailored DD sequence suppressing all interactions up to weight three, we can generate an orthogonal array using the projective geometry code \mathcal{C} and its dual (also known as the simplex code) as \mathcal{C}^\perp . The code is chosen because it enables large chromatic number χ_I using minimal number of generators, resulting in a highly time-efficient sequence.

This section is organized as follows. We begin by briefly reviewing the construction of linear and additive codes based on projective geometry with distances $d = 3$ and $d = 4$. We then show how to modify these codes to tailor them to the spin-qubit platform.

1. Linear projective geometry code

A projective geometry space $\text{PG}(n, q)$ is the set of equivalence classes in the vector space $\mathbb{F}_q^{n+1}/\{\mathbf{0}\}$ of which two vectors $\mathbf{u}, \mathbf{v} \in \mathbb{F}_q^{n+1}$ belong to the same equivalence class $[\mathbf{u}]$ if they differ by scalar multiplication, i.e. $\mathbf{u} = \alpha \mathbf{v}$ for some $\alpha \in \mathbb{F}_q$. Consequently, one can view each point $[\mathbf{u}] \in \text{PG}(n, q)$ as a collection of points in \mathbb{F}_q^{n+1} starting from \mathbf{u} and passing through the origin.

The projective space that we will use to construct the decoupling group is $\text{PG}(n, 4)$. The decoupling group is constructed using the linear check matrix H of the linear code \mathcal{C} . As a reminder, the codeword $\mathbf{c} \in \mathcal{C}$ is the kernel of the check matrix, i.e.

$$H\mathbf{c} = \mathbf{0}. \quad (42)$$

As a first step, we show how to construct a decoupling group for universal cancellation of all two-body interactions from the projective space. We begin by choosing the columns of the check matrix H to correspond to points $[\mathbf{u}]$ in the projective space $\text{PG}(n, 4)$; that is, to equivalence classes of nonzero vectors in \mathbb{F}_4^{n+1} . The total number of such equivalence classes is given by

$$\frac{4^{n+1} - 1}{3}. \quad (43)$$

From the construction of the check matrix, it follows that the code distance is $d \geq 3$. To see this, we proceed by contradiction and assume that there exists a codeword \mathbf{c} with Hamming weight two. This implies the existence of two columns $[\mathbf{u}], [\mathbf{v}]$ that are linearly dependent, i.e.,

$$[\mathbf{u}] = \alpha[\mathbf{v}], \quad (44)$$

for some $\alpha \in \mathbb{F}_4$. However, by definition of projective space, all distinct points $[\mathbf{u}] \in \text{PG}(n, 4)$ are pairwise linearly independent. Thus, no such weight-two codeword can exist, and the minimum distance of the code must be at least three.

Because the check matrix H of the linear code \mathcal{C} is the linear (not additive) generator matrix for the dual code \mathcal{C}^\perp , using Theorem IV.1, we can construct an OA from \mathcal{C}^\perp with parameters

$$\text{OA}\left(4^{n+1}, \chi_I = \frac{4^{n+1} - 1}{3}, 4, 2\right). \quad (45)$$

As a result, the decoupling sequence derived from this orthogonal array universally decouples all two-local interaction terms.

We now show how to construct DD sequences that universally decouple all three-local interactions using linear projective geometry code. The key requirement is that the columns of the check matrix H must form a cap set. A cap set (also known as an arc in projective geometry) in $\text{PG}(n, 4)$ is a collection of points $[\mathbf{u}]$ such that no three are collinear. This condition ensures that the corresponding linear code \mathcal{C} has minimum distance $d = 4$, thereby detecting all weight-three errors.

Let n_H denote the number of columns in the check matrix, i.e. the size of the cap set. Then, the orthogonal array constructed from the dual code \mathcal{C}^\perp has parameters

$$\text{OA}(4^{n+1}, \chi_I = n_H, 4, 3). \quad (46)$$

An important remaining question is how to construct a cap set in $\text{PG}(n, 4)$ with the largest possible size. In general, this is a challenging problem in projective geometry. However, explicit constructions of maximal cap sets are known for small values of n [76]. For example, the largest cap set sizes for $n = 2, 3, 4$ are $n_H = 6, 17, 41$ respectively. For higher dimensions n , near-optimal constructions are known, although it is unlikely that physically relevant graphs of solid-state devices will require these large chromatic number χ_I .

2. Additive projective geometry code

In the preceding construction, we employed linear projective geometry codes to design universal DD groups for two-local and three-local interactions. We now show that if we use additive projective geometry codes [77], we can construct more time-efficient sequences. The key insight is that the field \mathbb{F}_4 , when considered under addition, is isomorphic to $\mathbb{F}_2 \times \mathbb{F}_2$. Exploiting this structure, Ref. [77] demonstrates that the check matrix H of an additive code with parameters $(\chi_I, 2^k, d)_4$ can be constructed from a collection of χ_I lines in the projective space $\text{PG}(2\chi_I - k - 1, 2)$, such that any $d - 1$ lines in the set are linearly independent.

To universally decouple two-local interactions, we require the code \mathcal{C} to have distance $d = 3$. Consequently, we need to choose a collection of χ_I lines in the projective space $\text{PG}(2\chi_I - k - 1, 2)$ such that any 2 lines in the set are linearly independent. This set is known in projective geometry as a (partial) 1-spread. The maximum logical dimension k is given by

$$k = 2\chi_I - h \quad (47)$$

where h is the smallest integer number such that $2^h \geq 3\chi_I + 1$ for even h , and $2^h \geq 3\chi_I + 5$ for odd h . As a result, the orthogonal array constructed from \mathcal{C}^\perp with H as the additive generator matrix has parameter

$$\text{OA}(2^{\lceil \log_2(3\chi_I+1) \rceil \setminus \lceil \log_2(3\chi_I+5) \rceil}, \chi_I, 4, 2). \quad (48)$$

As a simple example, Table II(a) lists a full 1-spread of the projective space $\text{PG}(3, 2)$, where each projective

line is represented by two projective points. Each line is further associated with a color class c_i . In Table II(b), we map each projective line in $\text{PG}(3, 2)$ to a projective point in $\text{PG}(3, 4)$ via a simple embedding from $\mathbb{F}_2 \times \mathbb{F}_2$ to \mathbb{F}_4

$$(0, 0) \rightarrow 0, (1, 0) \rightarrow 1, (0, 1) \rightarrow \omega, (1, 1) \rightarrow 1 + \omega. \quad (49)$$

The resulting rows in the table form generators of a decoupling group capable of suppressing arbitrary two-local interactions.

We note that the above construction uses the same number of color classes and length in the decoupling sequence as the multi-axis protocol introduced in Ref. [27]. This is not a coincidence. The multi-axis protocol can be understood as implicitly employing an additive code over \mathbb{F}_4 . This connection arises because the Hadamard matrix defines a binary linear code (the Hadamard code), whose rows or columns correspond to codewords. By grouping these rows into Schur sets [78] and mapping from $\mathbb{F}_2 \times \mathbb{F}_2$ to \mathbb{F}_4 , one preserves the additive structure of the binary code. Moreover, Ref. [33] shows in their work (under the name of Walsh functions) that with minor modifications, the same construction can be extended to enable universal quantum simulation. Consequently, our framework naturally includes the protocols from Ref. [27, 33], providing an alternative way to understand their underlying structure.

To universally decouple three-local interactions, we did not find any explicit constructions using additive projective geometry codes in the literature. However, we expect that additive codes could potentially yield slightly more efficient decoupling sequences for three-local interactions as well. We leave the development of such constructions as an interesting direction for future research.

3. Tailored sequences for spin-qubit

We have demonstrated that projective geometry codes enable efficient decoupling of both two-local and three-local interactions, applicable to bang-bang and bounded-control sequences alike. We now present a simplified, tailored construction that universally suppresses single-qubit errors while specifically removing the Heisenberg exchange and scalar chirality interactions, the naturally occurring residual many-body interactions in spin-qubit platforms.

Let us first focus on the two-body Heisenberg exchange interactions. The main idea is to modify the columns of the check matrix such that no codeword corresponds to a term in the Heisenberg exchange interaction. Specifically, no weight-two codeword of the form $[1, 1], [\omega, \omega], [1 + \omega, 1 + \omega]$ is allowed. In the linear projective geometry code construction, only one representative for each projective equivalence class $[\mathbf{u}]$ is used as a column in the check matrix. As an example, the three equivalent representations of $[(1, \omega)]$ are

$$[(1, \omega)] = \{(1, \omega), (\omega, 1 + \omega), (1 + \omega, 1)\} \quad (50)$$

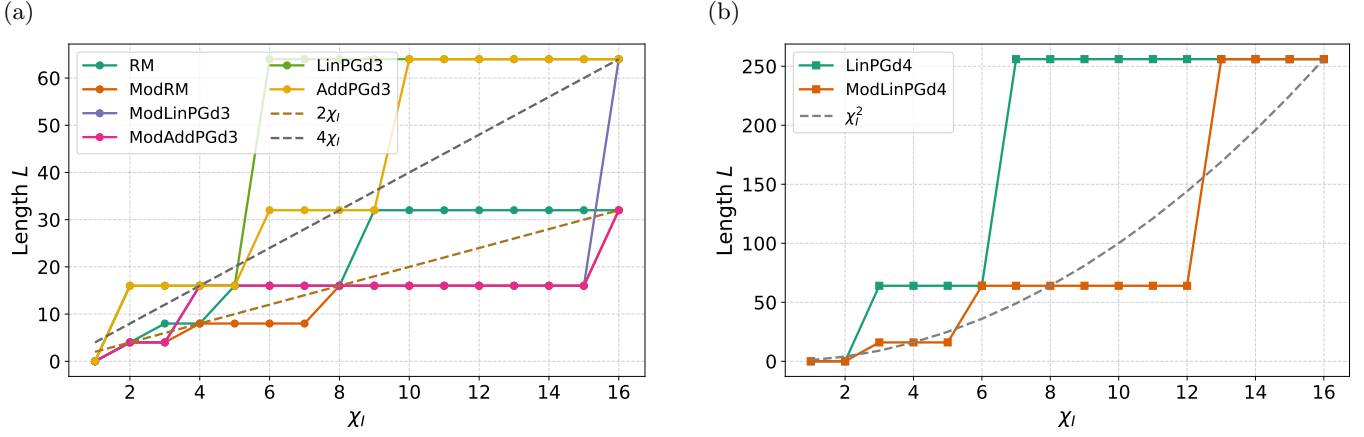


FIG. 7: **Scaling of decoupling sequences.** Scaling of sequence length L with the chromatic number χ_I for the code constructions listed in Table III. (a) For comparison, the linear baseline $L = 4\chi_I$ is shown in black. All codes with distance $d = 3$ exhibit linear scaling in χ_I , while those with $d = 4$ show quadratic scaling, consistent with the scaling reported in Ref. [32].

Scheme	# Gen.	2-local	3-local	Bounded
Mod. RM	$\lceil \log_2(\chi_I + 1) \rceil$	ZZ	–	Yes
RM	$\lceil \log_2(\chi_I) \rceil + 1$	ZZ	ZZZ	Yes
Lin-PG ($d = 3$)	$2 \log_4(3\chi_I + 1)$	All	–	Yes
Lin-PG ($d = 4$)	6, 8, 10*	All	All	Yes
Add-PG ($d = 3$)	$\log_2(3\chi_I + 1) \setminus \log_2(3\chi_I + 5)$	All	–	Yes
Mod. Lin-PG ($d = 3$)	$2 \log_4(\chi_I + 1)$	Hexch.	–	No
Mod. Lin-PG ($d = 4$)	4, 6, 8, 10**	Hexch.	Chir.	No
Mod. Add-PG ($d = 3$)	$\log_2(\chi_I + 1) \setminus \log_2(\chi_I + 5)$	Hexch.	–	No

TABLE III: **Comparison of decoupling sequences.** “# Gen.” indicates the number of additive code generators. “Hexch.” = Heisenberg exchange; “Chir.” = scalar chirality; “All” = universal decoupling. Asterisk values * and ** denote number of additive generators for $\chi_I = 6, 17, 41$ and $\chi_I = 5, 12, 34, 82$ respectively. “Bounded” indicates whether the scheme is compatible with bounded control (all work with bang-bang control).

The key observation is that if we include all projective points in the equivalence class $[\mathbf{u}]$ as separate columns of the check matrix H , no Heisenberg exchange terms arise as codewords. This effectively increases the number of allowed colors χ_I in the decoupling sequence by three times.

A similar strategy also applies to additive projective geometry codes: for each line in the projective space, there exist three distinct representations that also avoid Heisenberg exchange terms as codewords. As an illustration, Table II(c) presents a tailored DD group designed to suppress Heisenberg exchange interactions, derived from the construction in Table II(b). Notably, this construction increases the number of color classes from 5 to 15 while retaining the same number of generators. In the case of the multi-axis protocol introduced in Ref. [27], this modification is equivalent to cyclically permuting the rows in the Schur set.

When applying this straightforward extension to Fig. 6(b), under the assumption of residual Heisenberg exchange interactions, the tailored decoupling se-

quence still requires four generators, matching the number needed for a universal sequence that suppresses all two-local interactions. Therefore, for $\chi_I = 4, 5$ this basic approach does not yield a shorter sequence. However, in Appendix C, we present optimized tailored sequences for these specific cases that require only three generators, offering a reduction in sequence length.

Through exhaustive numerical search, we confirm that this extended construction yields a near-optimal number of color classes for decoupling at fixed sequence lengths $L = 16, 32$, and 64 . However, we note that shorter sequences, such as those of length $L = 4$ (i.e. Eq. (26)) and $L = 8$ are also possible, albeit supporting fewer color classes. Such compact sequences can be systematically constructed by iteratively removing one generator from DD group with longer sequence length L at a time and reducing the number of color classes, while ensuring that the resulting DD group still suppresses arbitrary single-qubit errors and detects Heisenberg exchange interactions.

When including the three-body scalar chirality inter-

action, a similar strategy can be applied to increase the number of allowed colors in the decoupling sequence. However, the additional constraints imposed by this interaction limit the modification of the projective geometry code's columns to only doubling the color count χ_I .

Let us apply this idea to the quotient hypergraph in Fig. 6(b). We begin by constructing a cap set in $\text{PG}(2, 4)$, which corresponds to a universal DD sequence that decouples all three-local interactions among six qubits. This cap set is given by the additive generators of the self-dual hexacode [79]

$$\begin{pmatrix} 1 & 0 & 0 & 1 & 1 & \omega \\ 0 & 1 & 0 & 1 & \omega & 1 \\ 0 & 0 & 1 & \omega & 1 & 1 \\ \omega & 0 & 0 & \omega & \omega & 1 + \omega \\ 0 & \omega & 0 & \omega & 1 + \omega & \omega \\ 0 & 0 & \omega & 1 + \omega & \omega & \omega \end{pmatrix}. \quad (51)$$

To construct a tailored sequence, we remove the first three columns and focus on the remaining three. We then apply the expansion strategy by selecting one of these columns (e.g. the last) and multiplying it by ω to generate a new fourth column

$$\begin{pmatrix} 1 & 1 & \omega & 1 + \omega \\ 1 & \omega & 1 & \omega \\ \omega & 1 & 1 & \omega \\ \omega & \omega & 1 + \omega & 1 \\ \omega & 1 + \omega & \omega & 1 + \omega \\ 1 + \omega & \omega & \omega & 1 + \omega \end{pmatrix} \rightarrow \begin{pmatrix} X & X & Z & Y \\ X & Z & X & Z \\ Z & X & X & Z \\ Z & Z & Y & X \\ Z & Y & Z & Y \\ Y & Z & Z & Y \end{pmatrix}. \quad (52)$$

The resulting DD sequence suppresses both the Heisenberg exchange interactions and the scalar chirality terms. However, it stills contains six generators. By mapping the generator set to a minimum covering problem, as described in Sec. IV D, we find that only four of these generators are necessary to suppress all relevant interaction terms

$$\begin{pmatrix} X & X & Z & Y \\ X & Z & X & Z \\ Z & Z & Y & X \\ Z & Y & Z & Y \end{pmatrix}. \quad (53)$$

Without going into detail, we also report that applying the same expansion strategy to one of the unused original columns (e.g., the first column) allows us to increase the number of interaction colors to $\chi_I = 5$ while still requiring only four generators

$$\begin{pmatrix} Z & X & X & Z & Y \\ Y & Z & X & X & Z \\ Y & Z & Z & Y & X \\ X & Y & Z & Z & Y \end{pmatrix}. \quad (54)$$

These optimized sequences achieves the same suppression with only $L = 16$ pulses, compared to a universal DD sequence of length $L = 64$, yielding a fourfold reduction in sequence length.

We emphasize that the expansion approach is effective primarily for bang-bang sequences. Under bounded control, finite pulse durations can lead to Heisenberg exchange or scalar chirality interactions transforming into other three-local terms that the sequence may not suppress. In such cases, alternative constructions may be required to obtain tailored, time-efficient bounded-control DD sequences. Alternatively, one may resort to the universal DD sequences discussed in Sec. VB 1, which, although potentially longer, suppress all three-local interactions. Finally, we note that shorter sequences can often be obtained by systematically removing generators from a universal sequence, one at a time, as demonstrated above. This process might reduce the number of supported color classes but preserving the required decoupling properties. Developing such compact, tailored sequences remains an interesting direction for future work.

For completeness, we summarize the parameters of all our constructions in Table III, along with their applicability to either bang-bang sequences or bounded-control sequences. Since all the sequences we consider permit universal DD, we only specify which types of two-local and three-local interactions are eliminated by each construction.

We also analyze the sequence lengths as a function of the chromatic number χ_I . To visualize this, in Fig. 7a we show the scaling of different DD sequences that suppress two-local interactions as the chromatic number χ_I increases; in Fig. 7b, we focus on sequences targeting three-local interactions. In both cases, we compare the scaling behavior of the sequence lengths against ideal linear and quadratic scaling. For two-local interactions, we find that the universal constructions scale linearly with sequence length $4\chi_I$, while the tailored constructions scale more compactly with $2\chi_I$. In the case of three-local interactions, both universal and tailored constructions exhibit quadratic scaling $L \propto \chi_I^2$, but the tailored sequences have a smaller prefactor, leading to more efficient implementations. These scaling behaviors are consistent with those of Ref. [32].

C. Digital-analog simulation

In the previous section, we showed how to construct DD sequences that suppress residual interactions within the system and its environment. In this section, we demonstrate how such sequences can also be leveraged for Hamiltonian simulation and digital-analog quantum computing. For concreteness, we consider the Kitaev's honeycomb lattice toy model, described by the Hamiltonian [80]

$$H_{\text{comb}} = -\frac{J_x}{4} \sum_{\langle ij \rangle_r} X_i X_j - \frac{J_y}{4} \sum_{\langle ij \rangle_g} Y_i Y_j - \frac{J_z}{4} \sum_{\langle ij \rangle_b} Z_i Z_j, \quad (55)$$

where the sum is taken over the red (r), blue (b), and green (g) colored edges in Fig. 8a. This model is ex-

actly solvable by using a mapping to Majorana fermions and exhibits both gapped and gapless phases depending on whether the coupling strengths J_x, J_y, J_z satisfy the triangle inequality [80]. Here, we focus on simulating the system deep in the gapless phase, where $J_x = J_y = J_z = J$.

We assume that the native analog Hamiltonian of the spin qubit device comprises Heisenberg interactions

$$H_{\text{analog}} = \sum_{\langle ij \rangle} \frac{J}{4} (X_i X_j + Y_i Y_j + Z_i Z_j). \quad (56)$$

We aim to simulate the target Hamiltonian H_{comb} using H_{analog} . First, because the native interactions are isotropic, with XX , YY , and ZZ couplings have the same amplitude, we must design a DD group that selectively preserves only one type of interaction (either XX , YY , or ZZ) based on the edge label in the honeycomb lattice. Second, once the desired interaction type is isolated, we must flip the global sign of the Hamiltonian to convert the native antiferromagnetic coupling (positive J) into a ferromagnetic one (negative J).

As in previous sections, we begin by identifying the effective number of equivalence color classes in Kitaev's honeycomb model. If we were to universally decouple all interactions, the honeycomb lattice would be trivially 2-colorable. However, because we aim to selectively preserve certain interactions, the effective model becomes more complex.

In particular, due to the link-dependent interaction terms in the Hamiltonian, the symmetry of the model reduces the problem to an effective system involving six color classes. In Fig. 8a, we color the qubits that are equivalent under the translation symmetry of the honeycomb lattice. The resulting quotient hypergraph, formed by identifying these symmetry-equivalent sites, contains six color classes. There are three extra edges appear between opposite effective vertices, as shown in Fig. 8b.

To demonstrate the power of the effective graph in Fig. 8b, we use the simple algorithm presented in Sec. IV D to find the minimal decoupling group for the bang-bang sequence. We also explicitly construct a decoupling group for the bounded sequence, see Appendix D. Using the same terminology as before, we associate $H_S^{\parallel} = H_{\text{comb}}$. Consequently, the remaining interactions belong to the list H_S^{\perp} .

By finding the kernel of the linear map defined in Eq. (32), we identify four operators spanning the kernel space that commute with H_S^{\parallel} . These operators are

$$W_1 = Z_1 X_2 Z_3 X_4, \quad W_2 = X_3 Z_4 X_5 Z_6, \quad (57a)$$

$$W_3 = Y_1 Y_3 X_5 X_6, \quad W_4 = Y_2 X_3 X_4 Y_5, \quad (57b)$$

and are closely related to a known symmetry of the Kitaev honeycomb model, namely the plaquette operators [80]

$$W_{p,1} = Z_1 X_2 Y_3 Y_4 X_5 Z_6, \quad W_{p,2} = Y_1 Y_2 Z_3 X_4 Z_5 X_6 \quad (58)$$

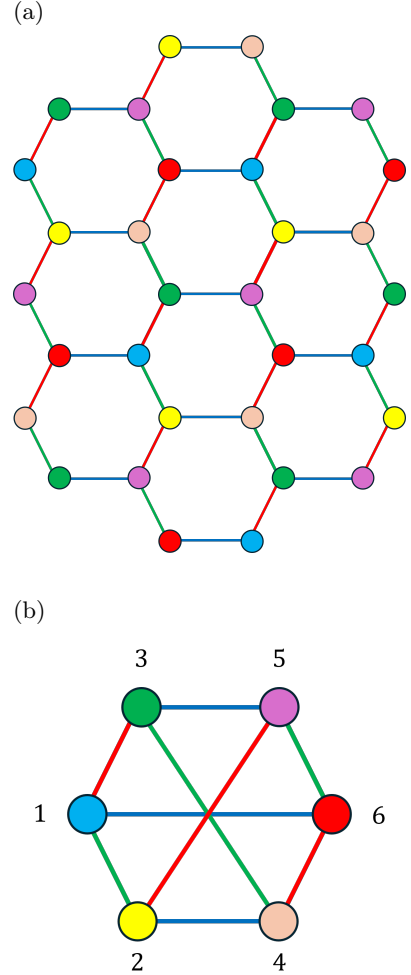


FIG. 8: **Dynamical quantum simulation of the Kitaev model.** (a) A finite-size Kitaev honeycomb lattice, where edges are colored red, green, and blue to represent $X_i X_j$, $Y_i Y_j$, and $Z_i Z_j$ interactions, respectively. The labels 1 through 6 indicate the equivalence classes of qubits under the vertex color partition which respects the edges coloring, not individual physical qubits. (b) The folded Kitaev lattice (i.e., the quotient hypergraph) obtained by collapsing all qubits within the same equivalence class. Compared to the standard unit cell, the quotient hypergraph includes three additional edges (2-5), (3-4), and (1-6) that arise from the folding.

One can verify that $W_1 W_2 = W_{p,1}$ and $W_3 W_4 = W_{p,2}$, that is, each pair provides a decomposition of the original plaquette symmetry. The emergence of these subsymmetries is expected: since the effective Kitaev honeycomb model arises from folding the original lattice, it can exhibit additional symmetries not present in the unfolded geometry.

If we take $W_{p,1}$ as the generator of \mathcal{G} , the resulting sequence effectively removes the interaction terms along the outer edges of the hexagon in Fig. 8b, aligning the

system's dynamics with that of the Kitaev model. However, the inner-edge interactions commute with $W_{p,1}$, so they are not eliminated by this sequence and remain in the effective Hamiltonian. This again reflects the presence of the subsymmetries introduced by lattice folding. In a similar manner, if we take $W_{p,2}$ as the generator of \mathcal{G} , there are interactions on outer edges that commute with $W_{p,2}$.

Either by numerically solving the associated minimum-set covering problem or by manually verifying it, we find that using either the pair (W_1, W_2) or (W_3, W_4) as generators is sufficient to construct a DD group \mathcal{G} for the bang-bang sequence. Consequently, the effective Hamiltonian have the same interaction as shown in the edges of Fig. 8b. However, the global sign is opposite of what it should be, i.e. $H_S^{\parallel} = -H_{\text{comb}}$.

To flip the global sign of the Hamiltonian, we use the following three operators

$$X_1 X_4 X_5, Y_1 Y_4 Y_5, Z_1 Z_4 Z_5. \quad (59)$$

Each of these operators commutes only with edges involving the same type of Pauli interaction and anti-commutes with the rest. For instance, $X_1 X_4 X_5$ commute with $X_1 X_3$ but anti-commutes with $Z_1 Z_2$. Consequently, by sequentially conjugating the effective Hamiltonian H_S^{\parallel} with these operators, we flip the sign of H_S^{\parallel} , yielding the target Kitaev Hamiltonian:

$$\sum_{P \in \{X, Y, Z\}} P_1 P_4 P_5 H_S^{\parallel} P_1 P_4 P_5 = H_{\text{comb}}. \quad (60)$$

Alternatively, we can view the three operators in Eq. (59) as (almost) forming a group. By including the identity operator, they generate the group

$$\langle X_1 X_4 X_5, Z_1 Z_4 Z_5 \rangle. \quad (61)$$

Twirling over the full group (including the identity) would suppress H_S^{\parallel} entirely. However, omitting the identity from the twirling set leads to the desired sign-flipping behavior described above. In conclusion, a full DD cycle implementing this sign-flipping mechanism consists of three such conjugations, each comprising a 4-element DD sequence, resulting in a total sequence length of $L = 3 \times 4 = 12$.

In this section, we have demonstrated how to construct a bang-bang sequence that simulates Kitaev's honeycomb model using only Heisenberg exchange interactions. In Appendix D, we extend this construction to bounded-control sequences for the same task. While the bounded-control sequence is significantly longer, it offers the advantage of allowing independent tuning of the interaction strengths J_x, J_y and J_z through the appropriate choice of control pulses.

VI. DESIGNING ROBUST SEQUENCES

In the previous sections, we implicitly assumed that X, Y , and Z π -pulses can be implemented perfectly. In experiments, however, pulse imperfections are inevitable and can significantly degrade the performance of a DD sequence if left unaddressed. This section introduces two complementary strategies to mitigate such imperfections and enhance the robustness of our DD constructions. In Sec. VIA, we show how to reduce the total number of applied pulses in DD sequences derived from classical additive codes. By exploiting the freedom in choosing the generator set, we can substantially lower the pulse count and establish a lower bound on the minimum number of pulses required based on the code distance. In Sec. VIB, we go a step further by addressing the imperfections of the pulses. We demonstrate how proper scheduling of (π) and ($-\pi$) pulses, together with a mirror-sequence strategy, can suppress both propagated pulse errors and residual free-evolution errors stemming from imperfect decoupling. Finally, in Sec. VIC, we perform numerical simulations of the proposed DD sequences on the bilinear array shown in Fig. 3(a), including longitudinal and transverse coherent error as well as residual nearest- and next-nearest-neighbor interactions.

A. Minimizing the number of pulses

In this section, we present a method to minimize the number of pulses applied in each round of a DD sequence. Reducing the pulse count per round offers several benefits: it relaxes demands on classical control electronics, decreases the accumulation of pulse-induced errors and crosstalk, and mitigates heating effects on the chip caused by frequent pulse application. To achieve this, we introduce the canonical implementation of DD sequences based on an additive group \mathcal{G} generated by a set $\Gamma_{\mathcal{G}} = \{\gamma_i\}$, where each applied pulse corresponds to one of the group generators γ_i . In the canonical implementation, the problem of minimizing the number of pulses per round reduces to finding a generating set for \mathcal{G} with minimal Hamming weights. Using this correspondence, we show that the code distance d provides a tight lower bound on the minimum number of pulses required per round.

We define $\text{Cay}(\mathcal{G}, \Gamma_{\mathcal{G}})$ as the Cayley graph of the decoupling group \mathcal{G} with respect to the generating set $\Gamma_{\mathcal{G}}$ [32, 35]. Since we consider \mathcal{G} to be an additive group (i.e., a subgroup of the Abelian projective Pauli group), the resulting Cayley graph is undirected. Its vertices correspond to the group elements $g_i \in \mathcal{G}$, and an edge labeled by a generator $\gamma_k \in \Gamma_{\mathcal{G}}$ connects two vertices g_i and g_{i+1} if and only if

$$g_{i+1} = \gamma_k g_i \text{ or equivalently } \gamma_k g_{i+1} = g_i. \quad (62)$$

We define a canonical implementation of a DD sequence as any closed path on the Cayley graph

$\text{Cay}(\mathcal{G}, \Gamma_{\mathcal{G}})$ that visits each vertex exactly once, starting and ending at the identity element. In other words, a canonical implementation corresponds to a Hamiltonian cycle on $\text{Cay}(\mathcal{G}, \Gamma_{\mathcal{G}})$. Such a cycle can be specified by the ordered list of visited vertices (excluding the initial identity)

$$\{g_1, g_2, \dots, g_{L-1}, g_L = I\}. \quad (63)$$

In practice, the corresponding DD implementation takes the form

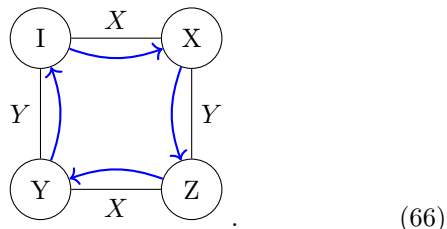
$$U_{\Delta}(g_{L-1}U_{\Delta}g_{L-1}) \dots (g_2U_{\Delta}g_2)(g_1U_{\Delta}g_1). \quad (64)$$

where each U_{Δ} denotes a free-evolution segment. Because the sequence follows a Hamiltonian cycle in the Cayley graph starting from the identity, the vertices obey

$$g_i \in \Gamma_{\mathcal{G}}, \quad \text{and} \quad g_{i+1}g_i \in \Gamma_{\mathcal{G}}. \quad (65a)$$

Thus, after combining adjacent pulses around each free-evolution interval in Eq. (64), the resulting canonical DD sequence contains only pulses drawn from the generating set $\Gamma_{\mathcal{G}}$.

As an illustrative example, let us revisit the $XY4$ sequence, which can be interpreted as a DD protocol generated from the single-qubit projective Pauli group. We take the generating set to be $\{X, Y\}$ rather than $\{X, Z\}$. The resulting Cayley graph is



The blue directed edges depict a Hamiltonian cycle on the graph corresponding to the standard implementation of the $XY4$ sequence. Each edge label denotes the generator applied to move between vertices, showing explicitly how the alternating application of X and Y pulses traverses the entire decoupling group.

To recap, we have defined canonical implementations of DD sequences. We now turn to the problem of minimizing the number of pulses applied per round. In a canonical implementation, each pulse corresponds to a generator γ_i of the additive group \mathcal{G} , so this problem reduces to minimizing the Hamming weight of these generators. As an example, consider the binary generator matrix of the $\text{RM}(1, 3)$ code shown in Table Ia. The first row of this matrix has weight 8, indicating that there exists a round in which control pulses must be applied simultaneously on all qubits. However, the choice of generator set $\Gamma_{\mathcal{G}}$ for the group \mathcal{G} is not unique. Any linear combination of the generators can serve as an alternative valid generating set. For instance, if $\{\gamma_1, \gamma_2, \gamma_3\}$ is a generator set, then $\{\gamma_1, \gamma_2 + \gamma_3, \gamma_1 + \gamma_3\}$ also generates the

same group. Applying this idea to Table Ia, we can construct an alternative generator matrix by replacing the first row with the sum of the first and second rows. The resulting generator matrix is

C_1	C_2	C_3	C_4	C_5	C_6	C_7	C_8
0	0	0	0	1	1	1	1
1	1	1	1	0	0	0	0
1	1	0	0	1	1	0	0
1	0	1	0	1	0	1	0

(67)

In the new generator matrix, the first generator has a Hamming weight of four, half that of the original, thereby reducing the number of simultaneous pulses required per round. This idea naturally extends to all DD sequences discussed in this work, since all our sequences are constructed from additive codes.

We now formally define the optimization problem of finding a generator matrix for the group \mathcal{G} with minimal Hamming weight. Let us start with an initial choice of generator matrix, which we also denote (by abuse of notation) as $\Gamma_{\mathcal{G}}$, whose rows γ_i are vectors over either \mathbb{F}_4 or \mathbb{F}_2 . We define a row-combination matrix R as an invertible square matrix with binary entries (0 or 1). An alternative, but equivalent, generator matrix $\bar{\Gamma}_{\mathcal{G}}$ for the same group \mathcal{G} can then be obtained as

$$\bar{\Gamma}_{\mathcal{G}} \equiv R\Gamma_{\mathcal{G}} \quad (68)$$

If we define $\text{Wg}(\Gamma_{\mathcal{G},i})$ as the Hamming weight of the i -th row of $\Gamma_{\mathcal{G}}$, the problem of minimizing the number of control pulses per round can be formulated as

$$\min_R \max_i \text{Wg}(R\Gamma_{\mathcal{G},i}). \quad (69)$$

In other words, the goal is to find the row-combination matrix R that minimizes the maximum weight among the generators, thereby reducing the number of simultaneous pulses required in a single round of the DD sequence.

We are not aware of any algorithms that efficiently solves Eq. (69), nor is its computational complexity established. A straightforward, though potentially suboptimal, choice for the generator matrix $\Gamma_{\mathcal{G}}$ is its standard form [81]. Nevertheless, a trivial lower bound on the minimum number of pulses per round can be inferred from the code properties of \mathcal{G} . Since \mathcal{G} defines an additive code, the minimum Hamming weight of any generator is bounded by the code distance d

$$\min_R \min_i \text{Wg}(R\Gamma_{\mathcal{G},i}) \geq d. \quad (70)$$

As an example, the new generator matrix of the $\text{RM}(1, 3)$ code in Eq. (67) achieves this bound, with all rows having the minimum possible Hamming weight. This observation implies that a robust DD sequence should be constructed from codes that balance two competing requirements: a high dual distance d^{\perp} to suppress high-weight errors, and a low distance d to minimize the number of pulses per round.

The discussion above implicitly assumes that each color class contains roughly the same number of qubits. If some color classes are significantly larger than others, Eq. (69) must be modified to account for the unequal distribution. In that case, the trivial lower bound in Eq. (70) becomes the product of the code distance d and the size of the smallest color class.

As a final remark, the flexibility in choosing the generator set can also be exploited for other optimization tasks. For example, common native physical single-qubit gates are the X - and Y -gates, while the Z -gate is typically virtual. Performing a physical Z -gate therefore requires a combination of X - and Y -gates, which increase gate errors. Consequently, one could construct an alternative generator matrix Γ_G that minimizes the use of Z -gates, reducing the overall pulse error. We leave this direction as future work.

B. Mitigating imperfect pulses

In the previous section, we have introduced the canonical implementation of DD sequences and discussed how to minimize the number of pulses applied per round. In this section, we turn to the complementary question of how to make these sequences robust against pulse imperfections. We present a simple and general strategy for implementing canonical DD sequences in a way that suppresses pulse errors. The key idea is based on two techniques: first, to schedule the (π) and $(-\pi)$ pulses so that their errors systematically cancel out (in the same spirit as the universal robust sequences of Ref. [82]); and second, to incorporate a mirror-sequence construction, analogous to how the standard $XY4$ sequence is extended to the more robust $XY8$ sequence. Together, these techniques provide a simple yet effective approach for mitigating pulse imperfections.

We start by rewriting the canonical DD sequence in Eq. (64) by grouping adjacent pulses

$$U_{\Delta} p_L \dots U_{\Delta} p_2 U_{\Delta} p_1. \quad (71)$$

Each pulse p_i is a tensor product of single-qubit Pauli operators

$$p_i = p_{i,1} \otimes p_{i,2} \dots \otimes p_{i,N} \in \Gamma_G \quad (72)$$

and is realized in practice by applying single-qubit gates $p_{i,k}$ in parallel across N qubits. We assume that the dominant source of pulse error is systematic over- or under-rotation. The case of misaligned rotation axes is more complicated and we discuss it in Appendix E. Under this assumption, the noisy implementations of θ -pulses for the k -th qubit in the i -th pulse are

$$(\tilde{p}_{i,k})_{\theta} \equiv \exp \left[-\frac{i}{2} \text{sign}(\theta)(\theta + 2\epsilon_{i,k})p_{i,k} \right], \quad (73a)$$

here $\epsilon_{i,k}$ captures the over- or under-rotation error. We assume that

$$|\epsilon_{i,k}| \leq \epsilon \quad \forall i, k \quad (74)$$

for small ϵ .

In this section, we consider two equivalent implementations of the $p_{i,k}$ gate, namely $\theta = \pi$ and $\theta = -\pi$ pulses. A noisy pulse \tilde{p}_i can then be written as a product of the ideal pulse p_i and a composite error operator $E[p_i]$ that accumulates all individual errors from each single qubit gates

$$\tilde{p}_i = E[p_i]p_i = \left(\prod_k e^{\pm i\epsilon_{i,k}p_{i,k}} \right) p_i, \quad (75)$$

where the sign of the rotation error depends on whether we apply the (π) or $(-\pi)$ -pulses. Accordingly, the noisy DD sequence becomes

$$U_{\Delta} E[p_L] p_L \dots U_{\Delta} E[p_1] p_1. \quad (76)$$

To analyze the effect of imperfect pulses, we commute the error operators $E[p_i]$ through the ideal pulses p_i and the free-evolution segment U_{Δ} . Our goal is to express the noisy DD sequence in Eq. (76) with the following form

$$\begin{aligned} & \left(\prod_{i=1}^L \tilde{E}[p_i] \right) U_{\Delta,L} p_L U_{\Delta,L-1} p_{L-1} \dots U_{\Delta,1} p_1 \\ & \equiv \left(\prod_{i=1}^L \tilde{E}[p_i] \right) e^{-i\Delta L(H_{\text{targ}} + H_{\text{error}})}. \end{aligned} \quad (77)$$

Here, $\tilde{E}[p_i]$ denotes the effective error operator obtained after commuting $E[p_i]$ through all subsequent ideal pulses p_j with $j > i$, while

$$U_{\Delta,i} \equiv \exp(-i\Delta H_{\text{eff},i}) \quad (78)$$

represents the modified free-evolution segment that incorporates the influence of all preceding errors $E[p_j]$ with $j \leq i$.

There are two distinct error types in Eq. (77). The first arises from the propagated pulse errors $\tilde{E}[p_i]$, which accumulate as the sequence proceeds. In Sec. VIB1, we show that these errors can be suppressed by appropriately scheduling (π) and $(-\pi)$ pulses so that their leading-order contributions cancel. The second originates from the residual error Hamiltonian H_{error} due to each free-evolution segment $U_{\Delta,i}$ evolves under a slightly different effective Hamiltonian. We address the suppression of the second error type in Sec. VIB2 using the mirror sequence.

1. Scheduling (π) and $(-\pi)$ -pulses

In this subsection, we show that errors due to $\tilde{E}[p_i]$ can be suppressed by an appropriate scheduling of (π) - and $(-\pi)$ -pulses within the canonical DD sequence. The key observation underlying this result is that in a canonical DD sequence, each generator γ_i appears an even number of time. By choosing the sign of the applied pulse (for

example, using a (π) -pulse the first time and a $(-\pi)$ -pulse the second), we can ensure that the first-order rotation errors introduced by these imperfect pulses cancel out, leaving only higher-order residual terms.

As a first step, we need to compute the exact form of $\tilde{E}[p_i]$. Since each error operator $E[p_i]$ is composed of independent single-qubit rotation errors (see Eq. (75)), we can analyze how each individual rotation error propagates through subsequent ideal pulses p_j . Consider commuting a single-qubit rotation error $e^{-i\epsilon_{ik}p_{i,k}}$ through a Pauli pulse p_j . Depending on whether the two Pauli operators commute or anticommute, the sign of the rotation angle may flip, converting an over-rotation into an under-rotation, or vice versa

$$p_j e^{-i\epsilon_{ik}p_{i,k}} = \begin{cases} e^{-i\epsilon_{ik}p_{i,k}} p_j & \text{if } [p_{i,k}, p_j] = 0, \\ e^{+i\epsilon_{ik}p_{i,k}} p_j & \text{otherwise} \end{cases}. \quad (79)$$

Therefore, the effective error operator $\tilde{E}[p_i]$ can be obtained by tracking how each local error term $e^{-i\epsilon_{ik}p_{i,k}}$ transforms under all subsequent ideal pulses p_j with $j > i$.

To formalize this, we define a commutation propagation function

$$\text{Com}(p_{i,k}, l) \equiv \begin{cases} (\prod_{j=i+1}^l p_j)^\dagger p_{i,k} (\prod_{j=i+1}^l p_j) & \text{for } l > i \\ p_{i,k} & \text{for } l = i \\ 0 & \text{otherwise} \end{cases} \quad (80)$$

which determines the final effective sign of a rotation error on k -th qubit from round i after propagating through the sequence up to round $l \leq L$. With the newly defined function, the full propagated error operator is given by

$$\tilde{E}[p_i] = \prod_k e^{\pm i\epsilon_{ik} \text{Com}(p_{i,k}, L)}, \quad (81)$$

where the \pm sign corresponds to whether the implemented pulse on the k -th qubit is a $(-\pi)$ - or (π) -rotation, respectively.

Expanding to first order in ϵ , the accumulated propagated pulse error can be approximated by keeping first order contribution in the Baker-Campbell-Hausdorff formula

$$\prod_{i=1}^L \tilde{E}[p_i] \approx \prod_k \exp \left[i \sum_{i=1}^L (\pm \epsilon_{ik}) \text{Com}(p_{i,k}, L) + O(\epsilon^2) \right]. \quad (82)$$

We note that when all the pulses $p_{i,k}$ acting on a given qubit commute with each other, as is the case for biased decoupling sequences, where only Z -type or only X -type pulses are predominantly applied, the above expression becomes exact rather than an approximation.

To achieve first-order cancellation of the propagated errors, it is sufficient that every operator $p_{i,k}$ appearing in the exponent has a matching counterpart $p_{j,k}$ (with $j \neq i$) that is identical

$$p_{i,k} = p_{j,k}. \quad (83)$$

Assuming this condition holds, we evaluate the signs of $\text{Com}(p_{i,k}, L)$ and $\text{Com}(p_{j,k}, L)$. If the signs of these two terms are identical, we apply a (π) -pulse for one and a $(-\pi)$ -pulse for the other. Conversely, if their signs are opposite, we apply the same pulse type, either both (π) or both $(-\pi)$. As a concrete example, by applying this pulse schedule to the XY4 sequence reproduces the known results [11, 12] that the standard implementation using a single pulse type, either all (π) pulses or all $(-\pi)$ pulses

$$U_\Delta(Y)_\pi U_\Delta(X)_\pi U_\Delta(Y)_\pi U_\Delta(X)_\pi \\ \text{or } U_\Delta(Y)_{-\pi} U_\Delta(X)_{-\pi} U_\Delta(Y)_{-\pi} U_\Delta(X)_{-\pi} \quad (84)$$

is more robust to pulse errors than alternating between (π) and $(-\pi)$ pulses.

Our final step is to show that in the canonical DD sequence, each generator γ_i necessarily appears an even number of times, ensuring that Eq. (83) can always be fulfilled. Since \mathcal{G} is an additive group, its Cayley graph $\text{Cay}(\mathcal{G}, \Gamma_{\mathcal{G}})$ is isomorphic to the hypercube graph $\mathbb{Z}_2^{|\Gamma_{\mathcal{G}}|}$. Accordingly, we can associate each vertex in $\text{Cay}(\mathcal{G}, \Gamma_{\mathcal{G}})$ with a binary coordinate in $\mathbb{Z}_2^{|\Gamma_{\mathcal{G}}|}$, and each generator γ_i with a unit basis vector \mathbf{e}_i . In a Hamiltonian cycle on the hypercube that starts and ends at the origin, every coordinate direction \mathbf{e}_i must be traversed an even number of times, half in the positive and half in the negative direction. Therefore, each generator γ_i appears an even number of times in the canonical implementation.

We remark that our strategy is simple yet broadly applicable to any DD sequence generated by an additive group. Nevertheless, once a specific DD sequence is chosen, there remains significant room for further optimization. For example, by carefully arranging the order in which the generators γ_i appear, it may be possible to achieve error cancellation beyond the first order [83]. An interesting direction would be to employ evolutionary ML methods to find the optimal Hamiltonian cycle [36]. We leave this avenue for future work.

2. Mirror sequence

In the previous subsection, we addressed how to mitigate propagated pulse errors $\tilde{E}[p_i]$. Assuming that the canonical DD sequence is implemented using the (π) and $(-\pi)$ pulse schedule described in Sec. VIB1, Eq. (77) can be approximated as

$$U_\Delta \tilde{p}_L \dots U_\Delta \tilde{p}_2 U_\Delta \tilde{p}_1 \approx e^{-i\Delta L (H_{\text{target}} + H_{\text{error}})}, \quad (85)$$

where the only remaining error arises from the fact that each free-evolution segment evolves under a slightly different effective Hamiltonian, giving rise to a residual error Hamiltonian H_{error} . In this section, we introduce the mirror sequence, which is directly analogous to the construction that promotes the XY4 sequence to the XY8 sequence [11]. We show that the mirror sequence suppresses H_{error} to first order in ϵ , at the cost of doubling the sequence length.

As a first step, we analyze the effect of pulling all the pulse errors $E[p_i]$ from inside Eq. (76) to the left-hand side, as done in Eq. (77). The effect of commuting the pulse error $E[p_i]$ through the free-evolution segment U_Δ is given by

$$e^{-iH_{\text{tot}}\Delta}E[p_i] = E[p_i]e^{-i(E[p_i]^\dagger H_{\text{tot}} E[p_i])\Delta}, \quad (86)$$

This shows that each free-evolution segment effectively evolves under a slightly modified Hamiltonian due to pulse imperfections. Assuming that the rotation errors $\epsilon_{i,k}$ are small, the exponent on the RHS of Eq. (86) can be expanded to first order in ϵ as

$$E[p_i]^\dagger H_{\text{tot}} E[p_i] \approx H_{\text{tot}} + i \sum_k (\pm\epsilon_{i,k}) [p_{i,k}, H_{\text{tot}}]. \quad (87)$$

A key observation is that the residual error on the right-hand side is additive to first order in ϵ , i.e.

$$E[p_j]^\dagger E[p_i]^\dagger H_{\text{tot}} E[p_i] E[p_j] \approx H_{\text{tot}} + i \sum_k (\pm\epsilon_{i,k}) [p_{i,k}, H_{\text{tot}}] + i \sum_k (\pm\epsilon_{j,k}) [p_{j,k}, H_{\text{tot}}]. \quad (88)$$

As a result, using Eq. (87) and accounting for the sign flips that occur when propagating the pulse errors $E[p_i]$ through the ideal pulses p_j (as discussed in Sec. VIB1), we find that the effective Hamiltonian during the l -th free-evolution segment is approximately

$$H_{\text{eff},l} \approx H_{\text{tot}} + \sum_{i=1}^l \sum_k (\pm\epsilon_{i,k}) [\text{Com}(p_{i,k}, l), H_{\text{tot}}]. \quad (89)$$

This expression makes explicit that each effective free-evolution operator $U_{\Delta,l}$ contains contributions from imperfect pulses applied at all earlier times. Consequently, after completing one imperfect canonical DD sequence, the net evolution is governed by an effective Hamiltonian H_{eff} that can be decomposed into the desired target Hamiltonian H_{targ} , which we seek to retain, and the residual error Hamiltonian H_{error} .

$$H_{\text{eff}} \equiv H_{\text{targ}} + H_{\text{error}} = \sum_{l=1}^L \frac{g_l H_{\text{eff},l} g_l}{L} \approx H_{\text{targ}} + \frac{1}{L} \sum_{l=1}^L g_l \left(\sum_{i=1}^l \sum_k (\pm\epsilon_{i,k}) \times [\text{Com}(p_{i,k}, l), H_{\text{tot}}] \right) g_l. \quad (90)$$

To suppress the residual evolution generated by H_{error} , we append a mirror sequence in which the pulses and the evolution segments appear in the reverse order

$$U_\Delta p_L \dots U_\Delta p_1 \xrightarrow{\text{Mirror sequence}} p_1 U_\Delta \dots p_L U_\Delta \quad (91)$$

For instance, applying the mirror sequence to the XY4 sequence in Eq. (84) leads to the robust (and symmetric)

XY8 sequence

$$\left[(X_\pi) U_\Delta (Y)_\pi U_\Delta (X)_\pi U_\Delta (Y)_\pi U_\Delta \right] \left[U_\Delta (Y)_\pi \times U_\Delta (X)_\pi U_\Delta (Y)_\pi U_\Delta (X)_\pi \right] \quad (92)$$

To explain why appending a mirror sequence can suppresses H_{error} , we rewrite the noisy mirror DD sequence in the form

$$\tilde{p}_1 U_\Delta \dots \tilde{p}_L U_\Delta \equiv e^{-i\Delta L (H_{\text{targ}} + H_{\text{error}}^{\text{mirror}})} \left(\prod_{i=1}^L \tilde{E}[p_i] \right), \quad (93)$$

where all pulse errors $E[p_i]$ are propagated to the right-hand side, in contrast to the left-propagation used in Eq. (77). Recall that, with the appropriate scheduling of (π) - and $(-\pi)$ -pulses, the accumulated pulse-error operator satisfies $\left(\prod_{i=1}^L \tilde{E}[p_i] \right) \approx I$ to first order in ϵ . Due to the reversed direction in which the pulse errors $E[p_i]$ are commuted through the mirror sequence, it is straightforward to show that

$$H_{\text{error}}^{\text{mirror}} = -H_{\text{error}}. \quad (94)$$

As a result, the residual error Hamiltonian $H_{\text{error}}^{\text{mirror}}$ generated by the mirror sequence cancels the residual error Hamiltonian H_{error} from the original sequence in Eq. (85). Although this derivation relies on the first-order Magnus expansion and therefore demonstrates cancellation only to first order in Δ , the overall symmetric structure of the combined sequence and its mirror (see Eq. (92)), together with the locality of the noise model, ensures that all errors are suppressed to second order in Δ .

We emphasize that using the (π) and $(-\pi)$ pulse schedule described in Sec. VIB1 is essential for error cancellation. Without this specific scheduling, the combined noisy DD sequence and its mirror take the form

$$e^{-i\Delta L (H_{\text{targ}} - H_{\text{error}})} \left(\prod_{i=1}^L \tilde{E}[p_i] \right)^2 e^{-i\Delta L (H_{\text{targ}} + H_{\text{error}})} \quad (95)$$

which, in general, does not lead to cancellation of over- and under-rotation errors.

C. Numerical simulation

As a proof of principle for the proposed robust sequence design, we consider the seven-qubit bilinear array shown in Fig. 3a. In the rotating frame of the qubits, we assume the system is subject to an always-on Hamiltonian

$$\sum_i (\delta\omega_{z,i} Z_i + \delta\omega_{x,i} X_i + \delta\omega_{y,i} Y_i) + \sum_{d(i,j)=1} J_{ij} Z_i Z_j + \sum_{d(i,j)=2} K_{ij} Z_i Z_j \quad (96)$$

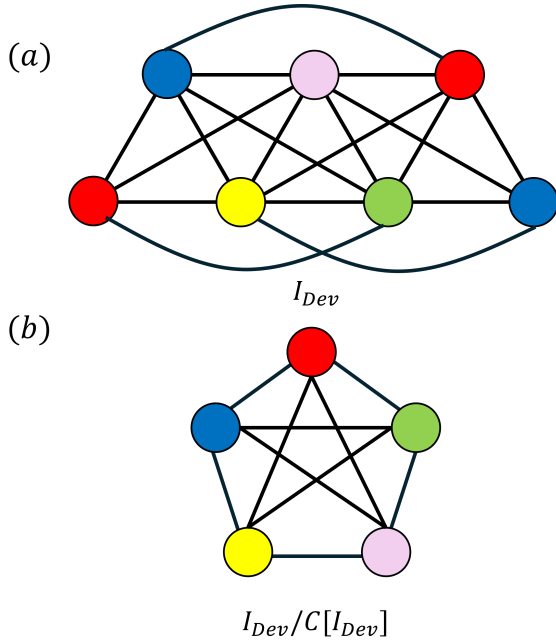


FIG. 9: **Interaction and quotient hypergraph of bilinear array** (a) Interaction hypergraph I_{Dev} of the device presented in Fig. 3(a) but with nearest- and next-nearest neighbor interactions, along with the minimal color partition $C[I_{Dev}]$. (b) The resulting quotient hypergraph $I_{Dev}/C[I_{Dev}]$ which is a simply fully connected pentagon.

which models longitudinal coherent error $\{\omega_{i,z}\}$, transversal coherent error $\{\omega_{i,x}, \omega_{i,y}\}$, residual nearest-neighbor interactions $\{J_{ij}\}$, and next-nearest-neighbor interactions $\{K_{ij}\}$. With the above Hamiltonian, the corresponding interaction hypergraph I_{Dev} and its quotient hypergraph $I_{Dev}/C[I_{Dev}]$ are given in Fig. 9.

We assume a simple error model in which the typical interaction strengths satisfy

$$\delta\omega_{z,i} \sim \delta\omega_{x,i} \sim \delta\omega_{y,i} \sim J_{ij} \sim 1 \text{ MHz}, \quad K_{ij} \sim 0.1 \text{ MHz}. \quad (97)$$

Systematic single-qubit over-rotation or under-rotation errors $\epsilon_{i,k}$ are taken to be independently and uniformly distributed over the interval $[-5^\circ, 5^\circ]$. These errors may vary between different realizations of the DD sequence but are fixed within each realization. After completing each DD sequence, we compute the trace fidelity with respect to the identity operation

$$F \equiv \left| \frac{\text{Tr}(U_{DD})}{2^7} \right|^2 \quad (98)$$

which quantifies how effectively the sequence suppresses the unwanted dynamics. We compare the resulting fidelities for four cases: (i) no dynamical decoupling, (ii) the standard XY4 sequence, (iii) the XY8 sequence, (iv) the punctured RM(1,3) sequence listed in Table Ic (i.e the first five columns), and (v) its robust implementation. The robust RM(1,3) sequence is applied once, while the

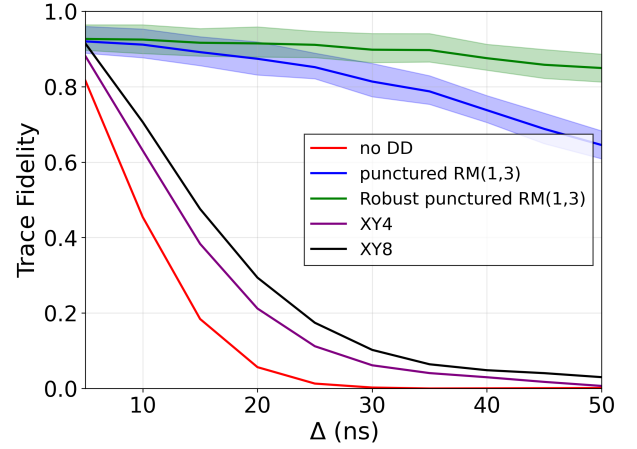


FIG. 10: **Trace fidelity of different DD sequences.** The mean value of trace fidelity as a function of the free-evolution segment duration $\Delta \in [5, 50]$ ns (in step of 5 ns) for the seven-qubit bilinear array shown in Fig. 3(a), subject to the error Hamiltonian in Eq. (96). We compare four cases: no dynamical decoupling (red), the standard XY4 sequence (purple), the punctured RM(1,3) sequence (blue), and its robust implementation (green). All sequences are applied for the same total evolution time. Each data point is averaged over 200 Monte Carlo realizations. Shaded regions indicate the interquartile range ($\pm 25\%$) around the mean trace fidelity. Surprisingly, we find that the quartile range for the red, purple, and black curves are small and thus not visible on the plot.

other sequences are repeated an appropriate number of times so that the total evolution time is identical across all cases (for example, repeating the XY4 sequence four times).

For each value of Δ ranging from 5 ns to 50 ns in step of 5 ns, we perform 200 Monte Carlo realizations. The results are shown in Fig. 10. Without dynamical decoupling, the accumulated errors rapidly scramble the qubit state. While the XY4 sequence suppresses single-qubit longitudinal and transversal coherent error, residual two-qubit interactions still lead to significant fidelity decay. We further observe that although the XY8 sequence improves the trace fidelity, it still exhibits an exponential decay due to these residual two-qubit interactions. In contrast, the punctured RM(1,3) DD sequence fully suppresses all error terms in the Hamiltonian of Eq. (96). Finally, we observe that the robust implementation of the RM(1,3) DD sequence yields a substantial improvement in trace fidelity as the segment duration Δ increases, in agreement with the arguments presented above.

In summary, by combining pulse scheduling with the mirror sequence, we achieve first-order suppression in the pulse error amplitude ϵ and second-order suppression in the free-evolution time Δ at the cost of doubling the sequence length L .

VII. CONCLUSION AND OUTLOOK

In this work, we have introduced a unified framework for constructing dynamical decoupling (DD) sequences for quantum devices with arbitrary connectivity and general k -local noise models. We first showed that the task of suppressing k -local interactions can be substantially simplified by exploiting symmetries induced by noise locality. This reduction enables the construction of DD sequences whose length depends only on the device topology, rather than on the total system size. We then leveraged the connection between DD sequences and classical additive codes: when the decoupling group is a subgroup of the single-qubit Pauli group, DD sequences can be interpreted as quaternary error-detecting codes over \mathbb{F}_4 . This perspective provides a systematic route to identifying good DD sequences from well-studied classical codes. Finally, we demonstrated how the group structure of these sequences can be exploited to construct implementations that are robust against systematic pulse over- and under-rotation errors.

As concrete demonstrations of our framework, we constructed explicit, time-efficient DD sequences tailored to superconducting and spin-qubit platforms that selectively suppress arbitrary interactions up to three-body order. Beyond error mitigation, we showed that the same framework can be used to engineer effective Hamiltonians for digital-analog quantum simulation. In particular, we presented a practical scheme for simulating the Kitaev honeycomb model on spin-qubit architectures, illustrating both the flexibility and the broader applicability of our approach.

Several interesting directions remain open for future investigation. Our current constructions are based on DD groups that are subgroups of the Pauli group, which naturally support a mapping to additive codes over \mathbb{F}_4 . An important next step is to extend this framework to DD groups that are subgroups of the Clifford group [84, 85]. Such sequences could achieve symmetrization of the system dynamics [45, 84], and could become an additional tool for Hamiltonian simulation [30]. In fact, Ref. [85] is closely aligned in spirit with our work, leveraging the symmetries of specific spin-spin interactions to design efficient decoupling sequences based on single-qubit Clifford groups. Another natural and important question is to incorporate selective DD sequences into quantum gate operations. As demonstrated in our recent work [60], inserting an echo pulse within a quantum gate that selectively flips interaction terms can reduce gate infidelity by at least an order of magnitude. A systematic extension of our framework to general quantum operations may be possible by combining it with dynamically corrected gate protocols [86]. Finally, our present analysis is restricted to DD sequences with an explicit group structure and equally spaced pulses. However, more general DD protocols that lack a strict group structure and employ non-equidistant pulse timings have been shown to provide higher-order error suppression

with fewer pulses [15–17, 38], as well as the ability to engineer effective interaction strengths beyond simple on-off control [30, 34, 87, 88]. Extending our hypergraph-coloring-based approach to encompass these more general DD schemes remain an open question.

VIII. ACKNOWLEDGMENT

We thank members of the Bosco, Rimbach-Russ, Terhal, and Vandersypen groups for valuable discussions. We are grateful to Pablo Cova Fariña for pointing out that the Kitaev honeycomb model can be simulated using a dynamical decoupling sequence of length $L = 4$. We thank Yuning Zhang for helpful discussions on constructing robust dynamical decoupling sequences and for sharing his Mathematica code.

This research was supported by the EU through the H2024 QLSI2 project, by the Army Research Office under Award Number: W911NF-23-1-0110, and by NCCR Spin (grant number 225153). The views and conclusions contained in this document are those of the authors and should not be interpreted as representing the official policies, either expressed or implied, of the Army Research Office or the U.S. Government. The U.S. Government is authorized to reproduce and distribute reprints for Government purposes notwithstanding any copyright notation herein.

Appendix A: Bounded control sequence

In this appendix, we review the bounded-control scheme for dynamical decoupling sequences [35]. The key idea is that the control operations are generated by a set of generators of the decoupling group \mathcal{G} . The decoupling sequence is implemented by continuously and smoothly evolving between elements of \mathcal{G} via these generators, rather than through instantaneous (bang-bang) pulses.

Let $\Gamma_{\mathcal{G}} = \{\gamma_1, \dots, \gamma_m\}$ denote a generating set of the decoupling group \mathcal{G} . We assume that each generator $\gamma_j \in \Gamma_{\mathcal{G}}$ can be implemented over a uniform time interval Δ using a time-dependent control Hamiltonian $h_{\gamma_j}(t)$ such that

$$\gamma_j = \mathcal{T} \exp \left(-i \int_0^{\Delta} dt h_{\gamma_j}(t) \right). \quad (\text{A1})$$

In the bounded control scheme, the control propagator U_c follows a balanced cycle in $\text{Cay}(\mathcal{G}, \Gamma_{\mathcal{G}})$. A balanced cycle is defined as a closed path that traverses each edge labeled by generator γ_j exactly λ_j times, where λ_j is a positive integer. Since $\text{Cay}(\mathcal{G}, \Gamma_{\mathcal{G}})$ is a regular graph, such a cycle always exists, and its length is exactly $|L| = |\mathcal{G}|(\sum_j \lambda_j)$. For clarity, we denote $\Lambda = \sum_j \lambda_j$.

The control propagator U_c starts at the identity element of the group \mathcal{G} and evolves according to a path

$L = \{l_1, \dots, l_{|L|}\}$, where each $l_i \in \Gamma_{\mathcal{G}}$ specifies a generator. Due to the deterministic structure of the Cayley graph, each vertex admits a unique outgoing edge for a given generator, ensuring an unambiguous evolution along the path. The control propagator is defined piecewise over intervals of duration Δ as

$$U_c[(j-1)\Delta + \tau] = u_{l_j}(\tau)U_c[(j-1)\Delta], \quad (\text{A2})$$

where

$$u_{l_j}(\tau) = \mathcal{T} \exp\left(-i \int_0^\tau dt h_{l_j}(t)\right) \quad (\text{A3})$$

for $\tau \in [0, \Delta)$.

Using Eq. (6), the average Hamiltonian \bar{H} can be grouped into elements of the generating set $\Gamma_{\mathcal{G}}$, namely

$$\bar{H} = \Pi_{\mathcal{G}}(F_{\Gamma}(H)) \quad (\text{A4a})$$

where the channel $F_{\Gamma}(H)$ is defined as

$$F_{\Gamma}(H) = \left(\sum_{\gamma_j \in \Gamma} \frac{\lambda_j}{\Lambda \Delta} \int_0^\Delta dt u_{\gamma_j}^\dagger(t) H u_{\gamma_j}(t) \right). \quad (\text{A5})$$

As a result, the total length of the bounded-control sequence increases by an additional factor proportional to the number of generators in $\Gamma_{\mathcal{G}}$.

Since F_{Γ} is a trace-preserving quantum channel, it maps traceless Hamiltonians to traceless operators. Therefore, if $U_{\mathcal{G}}$ defines an irreducible representation of \mathcal{G} , the decoupling sequence $\Pi_{\mathcal{G}}$ also decouples $F_{\Gamma}(H)$. However, in the more general case where $U_{\mathcal{G}}$ is not irreducible, the decoupling is guaranteed only if $F_{\Gamma}(H)$ does not acquire components within the invariant subspace of $\Pi_{\mathcal{G}}$. Therefore, successful decoupling under bounded control requires designing both the decoupling group \mathcal{G} and its generator set $\Gamma_{\mathcal{G}}$ such that neither H nor $F_{\Gamma}(H)$ has support in the invariant subspace preserved by the bang-bang decoupling $\Pi_{\mathcal{G}}$.

Appendix B: Superconducting qubit (bounded control)

In the main text, we showed how to construct a bang-bang decoupling sequence tailored to superconducting qubits using the binary Reed-Muller code. In this appendix, we extend that construction to the bounded-control setting, demonstrating how the same code framework can be adapted when only finite-time control pulses are available.

As a first step, we describe how to implement the control pulses associated with the generators of the decoupling group in the quotient hypergraph $I'_{\text{Dev}}/C[I_{\text{Dev}}]$. Each generator $\gamma_i \in \mathcal{G}$ is a Pauli string of the form

$$\gamma_{p_i} = [\gamma_{p_i}]_1 \otimes \dots \otimes [\gamma_{p_i}]_{\chi_{\mathcal{G}}}, \quad (\text{B1})$$

where each element $[\gamma_{p_i}]_k$ acts on the k -th color class. To lift this operator from the quotient hypergraph back to the original interaction hypergraph, we impose that $[\gamma_{p_i}]_k$ acts uniformly on all qubits belonging to the color class c_k . That is, for each qubit $q_j \in c_k$, the same single-qubit Pauli operator $[\gamma_{p_i}]_k$ is applied.

We assume the control Hamiltonian used to implement γ_{p_i} is composed of local, single-qubit Pauli operators, and is given by

$$h_{\gamma_{p_i}}(t) = \sum_{c_k \in C[I_{\text{Dev}}]} \sum_{q_j \in c_k} A_k^{q_j}(t) [\gamma_{p_i}]_k^{(q_j)}, \quad (\text{B2})$$

where $[\gamma_{p_i}]_k^{(q_j)}$ denotes the local Pauli operator assigned to qubit $q_j \in c_k$ and $A_k^{q_j}(t)$ are the time-independent amplitude of the pulses. The pulse amplitudes are controlled such that

$$\gamma_{p_i} = \mathcal{T} \exp\left(-i \int_0^\Delta h_{\gamma_{p_i}}(t) dt\right). \quad (\text{B3})$$

The decomposition ensures that each control pulse can be executed using local, parallel single-qubit operations in a way that respects the color partition of the interaction hypergraph.

As an example, we show that, under the substitution $0 \rightarrow I$ and $1 \rightarrow X$, the bounded-control decoupling sequence constructed from the $RM(1, m)$ code continues to suppress all Z -type Pauli strings of weight up to three. Since the generators are all X -type Pauli strings, the control Hamiltonian implements rotations around the X -axis. As a result, due to the finite duration of the control pulses, the channel F_{Γ} rotates a Pauli Z operator into linear combination of Z and Y

$$Z \rightarrow \cos(\alpha)Z + \sin(\alpha)Y. \quad (\text{B4})$$

The key insight is that the Y Pauli operator remains detectable by the X -type generators, since X anticommutes with Y . Therefore, any nontrivial operator in the image of F_{Γ} still anticommutes with some generator in the decoupling group \mathcal{G} . As a result, \mathcal{G} not only eliminates all Z -type strings of weight three or less but also cancels their rotated counterparts generated by the bounded-control channel F_{Γ} thereby ensuring effective suppression even under bounded-control sequence.

For the universal bounded-control sequence constructed from the $RM(1, m)$ code, we cannot simply apply the substitution 0 with I or Z and 1 with X and Y as done in the main text. This is because, under these substitutions, the channel F_{Γ} generally maps any Z -type Pauli string into a linear combination of arbitrary Pauli strings of the same weight, involving any mixture of X, Y and Z . Consequently, some of these terms may commute with all generators of the decoupling group \mathcal{G} and therefore are not suppressed by the sequence. This highlights a key limitation of bounded-control schemes for universal decoupling: unless the decoupling group is carefully designed, the sequence may fail to eliminate all error terms.

To overcome this issue, we introduce an additional generator of the form

$$Z_{c_1} \otimes Z_{c_2} \otimes \cdots \otimes Z_{c_{\chi_I}}, \quad (\text{B5})$$

which applies a global Z operator to each color class. This operator commutes with all Z -type Pauli strings, meaning the corresponding control Hamiltonian does not introduce any unwanted interactions that would require further cancellation. Crucially, it anticommutes with any single-qubit X or Y operator acting on a color class, thereby enabling universal decoupling of single-qubit errors. As a result, the total length of the bounded-control decoupling sequence becomes

$$2^{\lceil \log_2(\chi_I+1) \rceil + 1} (\lceil \log_2(\chi_I + 1) \rceil + 1) \sim O(\chi_I \log \chi_I), \quad (\text{B6})$$

which scales linearly with the chromatic number χ_I , with only a logarithmic overhead arising from the bounded-control implementation.

Appendix C: Tailored sequence for two-local interactions in spin-qubit architecture with $\chi_I = 4, 5$

In this appendix, we discuss how to construct tailored sequence for two-local interactions in spin-qubit architecture with $\chi_I = 4, 5$ using only three generators. The construction is based on additive code in $\text{PG}(2, 2)$.

We begin by labeling the seven points in the projective plane $\text{PG}(2, 2)$ as follows

$$\begin{bmatrix} P_1 & (1, 0, 0)^T \\ P_2 & (0, 1, 0)^T \\ P_3 & (0, 0, 1)^T \\ P_4 & (1, 1, 0)^T \\ P_5 & (1, 0, 1)^T \\ P_6 & (0, 1, 1)^T \\ P_7 & (1, 1, 1)^T \end{bmatrix}. \quad (\text{C1})$$

Throughout this section, we represent a line in $\text{PG}(2, 2)$ by an ordered pair of points (P_i, P_j) . The requirement that the code detects the Heisenberg exchange interaction translates into the following constraints on pairs of lines (P_i, P_j) and (P_n, P_m)

$$P_i \neq P_n, \quad P_j \neq P_m, \quad (\text{C2a})$$

$$P_i + P_j \neq P_n + P_m. \quad (\text{C2b})$$

These constraints can be reformulated as a combinatorial problem reminiscent of a Sudoku puzzle. Consider a 7×7 table whose rows and columns are labeled by the points P_1 through P_7 . Each entry in the table is defined

as the sum of the corresponding row and column labels

	P1	P2	P3	P4	P5	P6	P7
P1		P4	P5	P2	P3	P7	P6
P2	P4		P6	P1	P7	P3	P5
P3	P5	P6		P7	P1	P2	P4
P4	P2	P1	P7		P6	P5	P3
P5	P3	P7	P1	P6		P4	P2
P6	P7	P3	P2	P5	P4		P1
P7	P6	P2	P4	P3	P5	P1	

(C3)

The problem then becomes finding the largest possible subset of table entries such that no row, column, or resulting entry value appears more than once. This ensures that the pairwise constraints on lines are satisfied. For small instances such as this 7×7 table, heuristic search algorithms can be used to efficiently find such maximal subsets.

One such solution is the following set of line triples

$$\{(P_1, P_2, P_4), (P_2, P_3, P_6), (P_3, P_4, P_7) \quad (\text{C4a})$$

$$, (P_4, P_6, P_5), (P_5, P_7, P_2)\}. \quad (\text{C4b})$$

Converting these lines back into their point coordinates in $\text{PG}(2, 2)$ and then into Pauli operators, we obtain the following set of additive generators for the tailored decoupling group:

$$\begin{array}{c|c|c|c|c} C_1 & C_2 & C_3 & C_4 & C_5 \\ \hline 1 & 0 & 0 & 0 & 1 \\ 0 & 1 & 1 & 0 & 0 \\ 0 & 0 & 1 & 1 & 0 \\ 0 & 1 & 1 & 0 & 1 \\ 1 & 1 & 0 & 1 & 1 \end{array} \rightarrow \begin{array}{c|c|c|c|c} C_1 & C_2 & C_3 & C_4 & C_5 \\ \hline X & I & Z & X & Y \\ Z & X & Z & Y & Z \\ I & Z & X & Z & Y \end{array} \quad (\text{C5})$$

It is straightforward to verify that this decoupling group universally suppresses all single-qubit terms as well as Heisenberg exchange interactions in systems with $\chi_I = 4$ or 5.

In general, finding the largest set of ordered point pairs in $\text{PG}(n, 2)$ that satisfy the constraints of Eqs. C2 is computationally difficult. In fact, this problem can be shown to be NP-hard, as it is a specific instance of the well-known 3-dimensional matching problem. Consequently, the simple expansion strategy presented in the main text should be viewed as a heuristic algorithm. While effective for small instances, it leaves significant room for optimization in larger settings.

Appendix D: Simulating Kitaev's honeycomb model with bounded control

For the bounded-control setting, however, additional terms can be generated through the channel F_Γ . Accounting for these terms, we numerically find that all four operators W_1, W_2, W_3 , and W_4 are required to fully decouple the undesired interactions. The resulting sequence removes all two-local terms except those in H_{comb} . Moreover, by tuning the control Hamiltonian appropriately, it

becomes possible to simulate an anisotropic Kitaev model with $J_x \neq J_y \neq J_z$, even if the native system Hamiltonian consists solely of Heisenberg exchange interactions. The total number of time slices in the bounded-control protocol is then given by

$$2^4 \times 4 = 64. \quad (\text{D1})$$

Appendix E: Sequence robustness under misaligned rotation axis

In Sec. VI of the main text, we assumed that the dominant pulse error arises from systematic over- or under-rotation and presented strategies for making DD sequences robust against such errors. In this appendix, we analyze the case in which the dominant pulse error instead originates from misalignment of the rotation axis, and we explain why the proposed strategies are ineffective against this type of pulse error.

As a concrete example, we consider a noisy implementation of the $(\tilde{X})_\theta$ pulse given by

$$(\tilde{X})_\theta \equiv \exp \left[-\frac{i}{2} \theta (\sqrt{1 - \eta_y^2 - \eta_z^2} X + \eta_y Y + \eta_z Z) \right], \quad (\text{E1})$$

where $\eta_y, \eta_z \ll 1$ quantify small deviations of the rotation axis away from the ideal X direction. As in the main text, we decompose the noisy pulse into an error operator $E[(X)_\theta]$ followed by an ideal $(X)_\theta$ pulse

$$(\tilde{X})_\theta = (X)_\theta E[(X)_\theta]. \quad (\text{E2})$$

To determine the explicit form of the error operator $E[(X)_\theta]$, we employ the following math trick. Consider

$$\exp(i\lambda H) \exp[-i\lambda(H + \eta)] = F(\lambda), \quad (\text{E3})$$

with $F(0) = I$. Differentiating both sides with respect to λ yields

$$\frac{dF(\lambda)}{d\lambda} = \exp(i\lambda H) (-i\eta) \exp[-i\lambda(H + \eta)] \quad (\text{E4a})$$

$$= \exp(i\lambda H) (-i\eta) \exp(-i\lambda H), F(\lambda), \quad (\text{E4b})$$

where, in going from the first to the second line, we have inserted the identity $I = e^{-i\lambda H} e^{i\lambda H}$ and used Eq. (E3). To first order in $|\eta|$, the solution at $\lambda = 1$ is given by the first-order Magnus expansion,

$$F(1) \approx \exp \left[-i \int_0^1 d\lambda (\exp[i\lambda H] \eta \exp[-i\lambda H]) \right]. \quad (\text{E5})$$

Applying this result to the present case, with the identifications

$$\exp[-i\lambda(H + \eta)] = (\tilde{X})_\theta, \quad \exp[-i\lambda H] = (X)_\theta, \quad (\text{E6})$$

and $\theta = \pi$, we obtain the error operator

$$E[(X)_\pi] \approx \exp \left[-i \left(-\eta_y Z + \eta_z Y \right) \right]. \quad (\text{E7})$$

Importantly, we find that the error operator associated with a noisy $(\tilde{X})_{-\pi}$ pulse is identical to that of a $(\tilde{X})_\pi$ pulse. To first order in the misalignment parameters η , we have

$$E[(X)_{-\pi}] \approx E[(X)_\pi]. \quad (\text{E8})$$

This result can be directly verified using the identity

$$I = (\tilde{X})_{-\pi} (\tilde{X})_\pi \quad (\text{E9a})$$

$$\approx \exp \left[i \left(-\eta_y Z + \eta_z Y \right) \right] \exp \left[-i \left(-\eta_y Z + \eta_z Y \right) \right] \quad (\text{E9b})$$

$$= I, \quad (\text{E9c})$$

where we have kept terms only to first order in η . The fact that $E[(X)_{-\pi}]$ coincides with $E[(X)_\pi]$ for axis-misalignment errors has important consequences. By contrast, for over- and under-rotation errors one finds $E[(X)_{-\pi}] = E[(X)_\pi]^\dagger$, a property that allows cumulative pulse errors \tilde{E} (given in Eq. (82)) to be canceled by alternating between (π) and $(-\pi)$ pulses, as discussed in Sec. VIB1. This cancellation mechanism, however, is absent for misaligned rotation axis errors. Consequently, alternating between (π) and $(-\pi)$ pulses is ineffective in this case, and suppressing the accumulated pulse error instead requires choosing a Hamiltonian cycle such that the exponent on the right-hand side of Eq. (82) vanishes.

Another important distinction arises in the commutation properties of the pulse error $E[(X)_\pi]$ through the ideal pulse $(X)_\pi$. For misaligned rotation axis errors, we find

$$(X)_\pi E[(X)_\pi] = E[(X)_\pi]^\dagger (X)_\pi \quad (\text{E10})$$

whereas for over- and under-rotation errors the corresponding relation is

$$(X)_\pi E[(X)_\pi] = E[(X)_\pi] (X)_\pi. \quad (\text{E11})$$

Owing to the property in Eq. (E10), the mirror-sequence strategy introduced in Sec. VIB2 can in fact be used to suppress the cumulative pulse errors \tilde{E} arising from axis misalignment. However, this modified commutation relation also leads to a crucial limitation. Repeating the reasoning following Eq. (93), one finds that the mirror sequence no longer cancels the residual Hamiltonian error H_{error} . More explicitly, for misaligned rotation-axis errors, if the noisy DD sequence takes the form

$$U_\Delta \tilde{p}_L \dots U_\Delta \tilde{p}_1 = \left(\prod_{i=1}^L \tilde{E}[p_i] \right) e^{-i\Delta L(H_{\text{targ}} + H_{\text{error}})}, \quad (\text{E12})$$

then the corresponding mirror sequence necessarily has the structure

$$\tilde{p}_1 U_\Delta \dots \tilde{p}_L U_\Delta = e^{-i\Delta L(H_{\text{targ}} - H_{\text{error}})} \left(\prod_{i=1}^L \tilde{E}[p_i] \right)^\dagger. \quad (\text{E13})$$

As a result, while the cumulative propagated pulse error $\left(\prod_{i=1}^L \tilde{E}[p_i]\right)$ cancel out, the residual Hamiltonian errors add up, preventing full error suppression.

In summary, for misaligned rotation-axis errors, the pulse-scheduling strategies presented in Sec. VIB1 are

no longer effective. The mirror-sequence extension discussed in Sec. VIB2 can partially suppress pulse errors, but it does not eliminate them entirely. Consequently, an additional strategy is required to fully mitigate errors due to rotation-axis misalignment. We do not identify a simple solution within the scope of this work and therefore leave this problem for future investigation.

-
- [1] E. L. Hahn, Spin echoes, *Phys. Rev.* **80**, 580 (1950).
- [2] S. Meiboom and D. Gill, Modified spin-echo method for measuring nuclear relaxation times, *Review of Scientific Instruments* **29**, 688 (1958).
- [3] A. Maudsley, Modified carr-purcell-meiboom-gill sequence for nmr fourier imaging applications, *Journal of Magnetic Resonance* (1969) **69**, 488 (1986).
- [4] A. Brinkmann, Introduction to average hamiltonian theory. i. basics, *Concepts in Magnetic Resonance Part A* **45**, e21414 (2016).
- [5] A. Brinkmann, Introduction to average hamiltonian theory. ii. advanced examples, *Journal of Magnetic Resonance Open* **23**, 100191 (2025).
- [6] D. Vitali and P. Tombesi, Using parity kicks for decoherence control, *Phys. Rev. A* **59**, 4178 (1999).
- [7] L. Viola and S. Lloyd, Dynamical suppression of decoherence in two-state quantum systems, *Phys. Rev. A* **58**, 2733 (1998).
- [8] L. Viola, E. Knill, and S. Lloyd, Dynamical decoupling of open quantum systems, *Physical Review Letters* **82**, 2417 (1999).
- [9] L.-M. Duan and G.-C. Guo, Suppressing environmental noise in quantum computation through pulse control, *Physics Letters A* **261**, 139 (1999).
- [10] T. Gullion, D. B. Baker, and M. S. Conradi, New, compensated carr-purcell sequences, *Journal of Magnetic Resonance* (1969) **89**, 479 (1990).
- [11] Z.-H. Wang, W. Zhang, A. M. Tyryshkin, S. A. Lyon, J. W. Ager, E. E. Haller, and V. V. Dobrovitski, Effect of pulse error accumulation on dynamical decoupling of the electron spins of phosphorus donors in silicon, *Phys. Rev. B* **85**, 085206 (2012).
- [12] Z.-H. Wang, G. de Lange, D. Ristè, R. Hanson, and V. V. Dobrovitski, Comparison of dynamical decoupling protocols for a nitrogen-vacancy center in diamond, *Phys. Rev. B* **85**, 155204 (2012).
- [13] J. R. West, B. H. Fong, and D. A. Lidar, Near-optimal dynamical decoupling of a qubit, *Phys. Rev. Lett.* **104**, 130501 (2010).
- [14] S. Pasini and G. S. Uhrig, Optimized dynamical decoupling for time-dependent hamiltonians, *Journal of Physics A: Mathematical and Theoretical* **43**, 132001 (2010).
- [15] G. S. Uhrig, Keeping a quantum bit alive by optimized π -pulse sequences, *Phys. Rev. Lett.* **98**, 100504 (2007).
- [16] Z.-Y. Wang and R.-B. Liu, Protection of quantum systems by nested dynamical decoupling, *Physical Review A—Atomic, Molecular, and Optical Physics* **83**, 022306 (2011).
- [17] W. Yang and R.-B. Liu, Universality of Uhrig dynamical decoupling for suppressing qubit pure dephasing and relaxation, *Physical review letters* **101**, 180403 (2008).
- [18] P. Szańkowski, G. Ramon, J. Krzywda, D. Kwiatkowski, *et al.*, Environmental noise spectroscopy with qubits subjected to dynamical decoupling, *Journal of Physics: Condensed Matter* **29**, 333001 (2017).
- [19] G. A. Álvarez and D. Suter, Measuring the spectrum of colored noise by dynamical decoupling, *Phys. Rev. Lett.* **107**, 230501 (2011).
- [20] G. A. Paz-Silva and D. A. Lidar, Optimally combining dynamical decoupling and quantum error correction, *Scientific reports* **3**, 1530 (2013).
- [21] A. Vezvae, V. Tripathi, M. Morford-Oberst, F. Butt, V. Kasatkin, and D. A. Lidar, *Demonstration of high-fidelity entangled logical qubits using transmons* (2025), [arXiv:2503.14472 \[quant-ph\]](https://arxiv.org/abs/2503.14472).
- [22] V. Tripathi, H. Chen, M. Khezri, K.-W. Yip, E. Levenson-Falk, and D. A. Lidar, Suppression of crosstalk in superconducting qubits using dynamical decoupling, *Phys. Rev. Appl.* **18**, 024068 (2022).
- [23] J. Qiu, Y. Zhou, C.-K. Hu, J. Yuan, L. Zhang, J. Chu, W. Huang, W. Liu, K. Luo, Z. Ni, *et al.*, Suppressing coherent two-qubit errors via dynamical decoupling, *Physical Review Applied* **16**, 054047 (2021).
- [24] B. Evert, Z. G. Izquierdo, J. Sud, H.-Y. Hu, S. Grabbe, E. G. Rieffel, M. J. Reagor, and Z. Wang, Syncopated dynamical decoupling for suppressing crosstalk in quantum circuits, *arXiv preprint arXiv:2403.07836* (2024).
- [25] J. S. Waugh, L. M. Huber, and U. Haeberlen, Approach to high-resolution nmr in solids, *Phys. Rev. Lett.* **20**, 180 (1968).
- [26] K. Agarwal and I. Martin, Dynamical enhancement of symmetries in many-body systems, *Physical Review Letters* **125**, 080602 (2020).
- [27] A. F. Brown and D. A. Lidar, Efficient chromatic-number-based multi-qubit decoherence and crosstalk suppression, *arXiv preprint arXiv:2406.13901* (2024).
- [28] P. Coote, R. Dimov, S. Maity, G. S. Hartnett, M. J. Biercuk, and Y. Baum, Resource-efficient context-aware dynamical decoupling embedding for arbitrary large-scale quantum algorithms, *PRX Quantum* **6**, 010332 (2025).
- [29] E. Hickman, X. Wu, and G. Quiroz, *Crosstalk-robust dynamical decoupling for bipartite-topology quantum processors* (2025), [arXiv:2506.18010 \[quant-ph\]](https://arxiv.org/abs/2506.18010).
- [30] J. Choi, H. Zhou, H. S. Knowles, R. Landig, S. Choi, and M. D. Lukin, Robust dynamic hamiltonian engineering of many-body spin systems, *Phys. Rev. X* **10**, 031002 (2020).
- [31] M. Rotteler and P. Wocjan, Equivalence of decoupling schemes and orthogonal arrays, *IEEE Transactions on Information Theory* **52**, 4171–4181 (2006).
- [32] A. D. Bookatz, M. Roetteler, and P. Wocjan, Improved bounded-strength decoupling schemes for local hamiltonians

- nians, *IEEE Transactions on Information Theory* **62**, 2881–2894 (2016).
- [33] M. Votto, J. Zeiher, and B. Vermersch, Universal quantum processors in spin systems via robust local pulse sequences, *Quantum* **8**, 1513 (2024).
- [34] F. Rajabi, S. Motlakunta, C.-Y. Shih, N. Kotibhaskar, Q. Quraishi, A. Ajoy, and R. Islam, Dynamical hamiltonian engineering of 2d rectangular lattices in a one-dimensional ion chain, *npj Quantum Information* **5**, 32 (2019).
- [35] L. Viola and E. Knill, Robust dynamical decoupling of quantum systems with bounded controls, *Phys. Rev. Lett.* **90**, 037901 (2003).
- [36] C. Tong, H. Zhang, and B. Pokharel, Empirical learning of dynamical decoupling on quantum processors, arXiv preprint arXiv:2403.02294 (2024).
- [37] A. Rahman, D. J. Egger, and C. Arenz, Learning how to dynamically decouple by optimizing rotational gates, *Physical Review Applied* **22**, 054074 (2024).
- [38] J. Zhang, B. Peng, Y. Wang, C. K. Cheung, G. Bian, A. M. Edmonds, M. Markham, Z. Zhao, D. B. R. Dasari, R. Peng, Y. Wei, and J. Wrachtrup, [Learning to steer quantum many-body dynamics with tree optimization \(2025\)](#), arXiv:2510.07802 [quant-ph].
- [39] F. Casas, Sufficient conditions for the convergence of the magnus expansion, *Journal of Physics A: Mathematical and Theoretical* **40**, 15001 (2007).
- [40] T. Mori, Floquet states in open quantum systems, *Annual Review of Condensed Matter Physics* **14**, 35 (2023).
- [41] A. Iserles, Expansions that grow on trees, *Not. Am. Math. Soc.* **49** (2002).
- [42] K. Khodjasteh and D. A. Lidar, Rigorous bounds on the performance of a hybrid dynamical-decoupling quantum-computing scheme, *Phys. Rev. A* **78**, 012355 (2008).
- [43] A. Parra-Rodriguez, P. Lougovski, L. Lamata, E. Solano, and M. Sanz, Digital-analog quantum computation, *Phys. Rev. A* **101**, 022305 (2020).
- [44] T. Mostafaie, F. M. Khiyabani, and N. J. Navimipour, A systematic study on meta-heuristic approaches for solving the graph coloring problem, *Computers & Operations Research* **120**, 104850 (2020).
- [45] P. Zanardi, Symmetrizing evolutions, *Physics Letters A* **258**, 77 (1999).
- [46] M. Stollsteimer and G. Mahler, Suppression of arbitrary internal coupling in a quantum register, *Phys. Rev. A* **64**, 052301 (2001).
- [47] A. S. Hedayat, N. J. A. Sloane, and J. Stufken, *Orthogonal arrays: theory and applications* (Springer Science & Business Media, 2012).
- [48] Orthogonal Arrays — neilsloane.com, <http://neilsloane.com/oadir/index.html>.
- [49] P. Delsarte, Four fundamental parameters of a code and their combinatorial significance, *Information and Control* **23**, 407 (1973).
- [50] M. F. Ezerman, S. Ling, and P. Sole, Additive asymmetric quantum codes, *IEEE Transactions on Information Theory* **57**, 5536 (2011).
- [51] R. C. Bose and D. K. Ray-Chaudhuri, On a class of error correcting binary group codes, *Information and control* **3**, 68 (1960).
- [52] D. Gorenstein and N. Zierler, A class of error-correcting codes in p^m symbols, *Journal of the Society for Industrial and Applied Mathematics* **9**, 207 (1961).
- [53] A. R. Calderbank, E. M. Rains, P. W. Shor, and N. J. A. Sloane, [Quantum error correction via codes over \$gf\(4\)\$ \(1997\)](#), arXiv:quant-ph/9608006 [quant-ph].
- [54] B. Zeng, A. Cross, and I. L. Chuang, Transversality versus universality for additive quantum codes, *IEEE Transactions on Information Theory* **57**, 6272 (2011).
- [55] J. Haah, Algebraic methods for quantum codes on lattices, arXiv preprint arXiv:1607.01387 (2016).
- [56] G. Burkard, T. D. Ladd, A. Pan, J. M. Nichol, and J. R. Petta, Semiconductor spin qubits, *Reviews of Modern Physics* **95**, 025003 (2023).
- [57] X. Xue, M. Russ, N. Samkharadze, B. Undseth, A. Sammak, G. Scappucci, and L. M. K. Vandersypen, Quantum logic with spin qubits crossing the surface code threshold, *Nature* **601**, 343 (2022).
- [58] A. Noiri, K. Takeda, T. Nakajima, T. Kobayashi, A. Sammak, G. Scappucci, and S. Tarucha, Fast universal quantum gate above the fault-tolerance threshold in silicon, *Nature* **601**, 338 (2022).
- [59] A. R. Mills, C. R. Guinn, M. J. Gullans, A. J. Sigillito, M. M. Feldman, E. Nielsen, and J. R. Petta, Two-qubit silicon quantum processor with operation fidelity exceeding 99%, *Science Advances* **8**, eabn5130 (2022).
- [60] M. T. Nguyen, M. Rimbach-Russ, L. M. Vandersypen, and S. Bosco, Single-step high-fidelity three-qubit gates by anisotropic chiral interactions, arXiv preprint arXiv:2503.12182 [10.1103/kp8s-py9m](https://arxiv.org/abs/2503.12182) (2025).
- [61] S. Geyer, B. Hetényi, S. Bosco, L. C. Camenzind, R. S. Eggli, A. Fuhrer, D. Loss, R. J. Warburton, D. M. Zumbühl, and A. V. Kuhlmann, Anisotropic exchange interaction of two hole-spin qubits, *Nature Physics* **20**, 1152 (2024).
- [62] J. Saez-Mollejo, D. Jirovec, Y. Schell, J. Kukucka, S. Calcaterra, D. Chrastina, G. Isella, M. Rimbach-Russ, S. Bosco, and G. Katsaros, [Exchange anisotropies in microwave-driven singlet-triplet qubits \(2024\)](#), arXiv:2408.03224 [cond-mat.mes-hall].
- [63] P. C. Fariña, D. Jirovec, X. Zhang, E. Morozova, S. D. Oosterhout, S. Reale, T.-K. Hsiao, G. Scappucci, M. Veldhorst, and L. M. K. Vandersypen, [Site-resolved magnon and triplon dynamics on a programmable quantum dot spin ladder \(2025\)](#), arXiv:2506.08663.
- [64] T.-K. Hsiao, P. Cova Fariña, S. D. Oosterhout, D. Jirovec, X. Zhang, C. J. van Diepen, W. I. L. Lawrie, C.-A. Wang, A. Sammak, G. Scappucci, M. Veldhorst, E. Demler, and L. M. K. Vandersypen, Exciton transport in a germanium quantum dot ladder, *Phys. Rev. X* **14**, 011048 (2024).
- [65] S. P. Pedersen, K. S. Christensen, and N. T. Zinner, Native three-body interaction in superconducting circuits, *Phys. Rev. Res.* **1**, 033123 (2019).
- [66] T. Menke, W. P. Banner, T. R. Bergamaschi, A. Di Paolo, A. Vepsäläinen, S. J. Weber, R. Winik, A. Melville, B. M. Niedzielski, D. Rosenberg, K. Serniak, M. E. Schwartz, J. L. Yoder, A. Aspuru-Guzik, S. Gustavsson, J. A. Grover, C. F. Hirjibehedin, A. J. Kerman, and W. D. Oliver, Demonstration of tunable three-body interactions between superconducting qubits, *Phys. Rev. Lett.* **129**, 220501 (2022).
- [67] C. Berke, E. Varvelis, S. Trebst, A. Altland, and D. P. DiVincenzo, Transmon platform for quantum computing challenged by chaotic fluctuations, *Nature communications* **13**, 2495 (2022).
- [68] P. Nation, H. Paik, A. W. Cross, and Z. Nazario, The IBM quantum heavy hex lattice, <https://www.ibm.com/>

- [quantum/blog/heavy-hex-lattice](#) (2021).
- [69] Google Quantum AI et al., Quantum error correction below the surface code threshold, *Nature* **638**, 920 (2025).
- [70] E. Abbe, A. Shpilka, and M. Ye, Reed–muller codes: Theory and algorithms, *IEEE Transactions on Information Theory* **67**, 3251 (2020).
- [71] S. Bosco and M. Rimbach-Russ, [Exchange-only spin-orbit qubits in silicon and germanium](#) (2024), [arXiv:2410.05461 \[cond-mat.mes-hall\]](#).
- [72] D. Sen and R. Chitra, Large- u limit of a hubbard model in a magnetic field: Chiral spin interactions and paramagnetism, *Phys. Rev. B* **51**, 1922 (1995).
- [73] M. J. Gullans and J. R. Petta, Protocol for a resonantly driven three-qubit toffoli gate with silicon spin qubits, *Phys. Rev. B* **100**, 085419 (2019).
- [74] J. Qi, Z.-H. Liu, and H. Xu, [Scalable multi-qubit intrinsic gates in quantum dot arrays](#) (2024), [arXiv:2403.06894 \[quant-ph\]](#).
- [75] V. John, C. X. Yu, B. van Straaten, E. A. Rodríguez-Mena, M. Rodríguez, S. Oosterhout, L. E. Stehouwer, G. Scappucci, S. Bosco, M. Rimbach-Russ, *et al.*, A two-dimensional 10-qubit array in germanium with robust and localised qubit control, [arXiv preprint arXiv:2412.16044](#) (2024).
- [76] Q. Fu, R. Li, L. Guo, and G. Xu, Large caps in projective space $pg(r,4)$, *Finite Fields and Their Applications* **35**, 231 (2015).
- [77] A. Blokhuis and A. Brouwer, Small additive quaternary codes, *European Journal of Combinatorics* **25**, 161 (2004).
- [78] D. Leung, Simulation and reversal of n -qubit hamiltonians using hadamard matrices, *Journal of Modern Optics* **49**, 1199 (2002).
- [79] J. H. Conway and N. J. A. Sloane, *Sphere packings, lattices and groups* (2013) vol. 290, Springer Science & Business Media.
- [80] A. Kitaev, Anyons in an exactly solved model and beyond, *Annals of Physics* **321**, 2 (2006), january Special Issue.
- [81] M. A. Nielsen and I. L. Chuang, *Quantum computation and quantum information* (Cambridge university press, 2010).
- [82] G. T. Genov, D. Schraft, N. V. Vitanov, and T. Halfmann, Arbitrarily accurate pulse sequences for robust dynamical decoupling, *Phys. Rev. Lett.* **118**, 133202 (2017).
- [83] A. M. Childs, Y. Su, M. C. Tran, N. Wiebe, and S. Zhu, Theory of trotter error with commutator scaling, *Phys. Rev. X* **11**, 011020 (2021).
- [84] C. Read, E. Serrano-Ensástiga, and J. Martin, Platonic dynamical decoupling sequences for interacting spin systems, *Quantum* **9**, 1661 (2025).
- [85] C. Read, E. Serrano-Ensástiga, and J. Martin, [Dynamical decoupling of interacting spins through group factorization](#) (2025), [arXiv:2506.15382 \[quant-ph\]](#).
- [86] K. Khodjasteh and L. Viola, Dynamically error-corrected gates for universal quantum computation, *Phys. Rev. Lett.* **102**, 080501 (2009).
- [87] D. Hayes, S. T. Flammia, and M. J. Biercuk, Programmable quantum simulation by dynamic hamiltonian engineering, *New Journal of Physics* **16**, 083027 (2014).
- [88] M. F. O’Keeffe, L. Horesh, J. F. Barry, D. A. Braje, and I. L. Chuang, Hamiltonian engineering with constrained optimization for quantum sensing and control, *New Journal of Physics* **21**, 023015 (2019).